

國立交通大學  
理學院 應用化學系碩士班  
碩士論文

Department of Applied Chemistry, College of Science  
National Chiao Tung University

Master of Science degree thesis



**Mass Spectrometric Methods for the Analysis of Metabolites  
in Metazoan and Human Samples**

開發質譜法偵測生物代謝體之方法及應用

研究生： 曾德瑋  
指導教授： 帕偉鄂本 博士  
陳月枝 博士

Student: Te-Wei Tseng  
Advisors: Dr Pawel L. Urban  
Dr Yu-Chie Chen

Hsinchu – July, 2012

**Mass Spectrometric Methods for the Analysis of Metabolites  
in Metazoan and Human Samples**

**開發質譜法偵測生物代謝體之方法及應用**

研究生： 曾德瑋

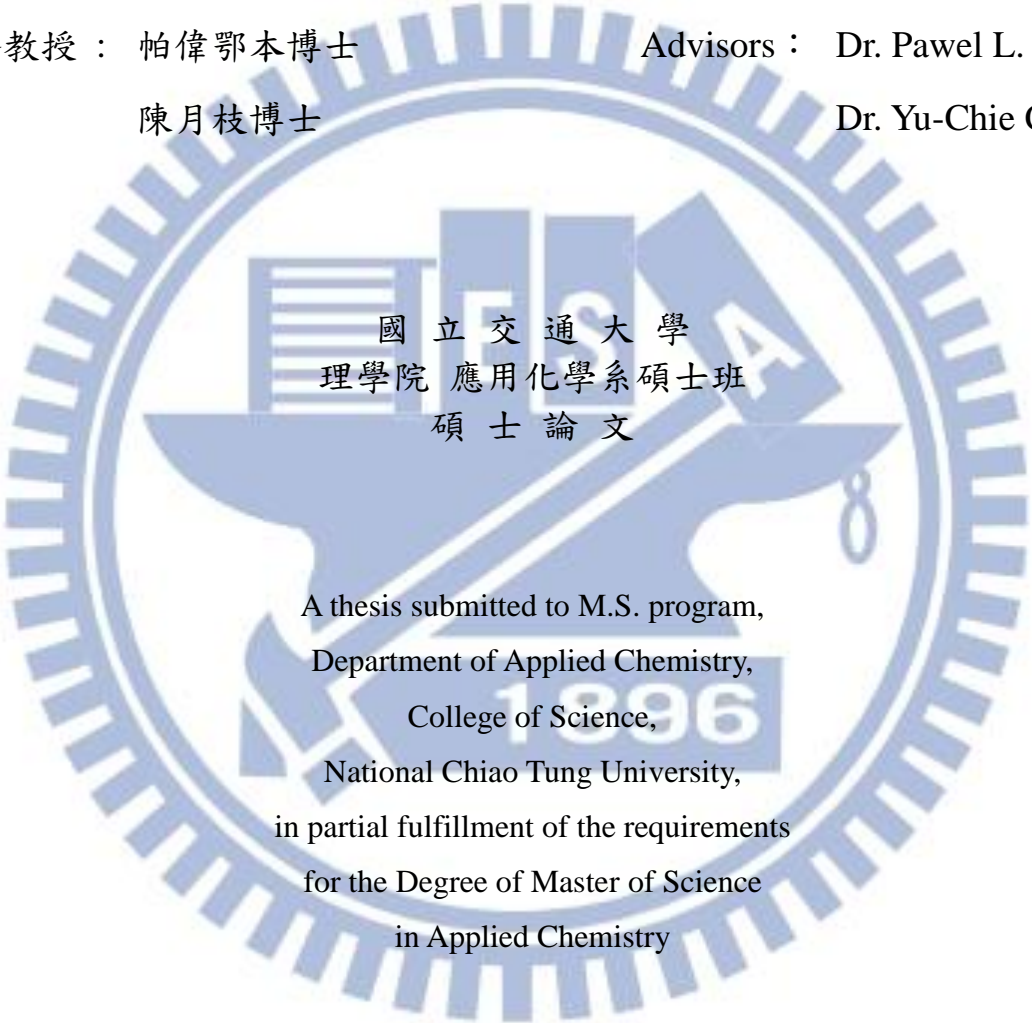
Student： Te-Wei Tseng

指導教授： 帕偉鄂本博士

Advisors： Dr. Pawel L. Urban

陳月枝博士

Dr. Yu-Chie Chen

The logo of National Chiao Tung University is a large, light blue circular emblem. It features a central design with a book, a graduation cap, and a gear. The text '國立交通大學' (National Chiao Tung University) is at the top, '理學院 應用化學系碩士班' (College of Science, Department of Applied Chemistry, Master's Program) is in the middle, and '碩士論文' (Master's Thesis) is at the bottom. The year '1896' is also visible at the bottom of the emblem.

國立交通大學  
理學院 應用化學系碩士班  
碩士論文

A thesis submitted to M.S. program,  
Department of Applied Chemistry,  
College of Science,  
National Chiao Tung University,  
in partial fulfillment of the requirements  
for the Degree of Master of Science  
in Applied Chemistry

July, 2012

Hsinchu, Taiwan, Republic of China

中華民國一百零一年七月

## ABSTRACT

In this work, we describe the development of two analytical methods based on mass spectrometry (MS), which are applicable to analysis of metabolites in biological samples: single eggs of fruit flies and human sweat. In the first part, we present mass spectrometric analysis of small metazoan (fruit fly) samples collected after *in-vivo* labeling with a stable isotope (carbon-13). We have found that matrix-assisted laser desorption/ionization (MALDI)-MS, used in conjunction with the isotopic labeling, enables quasi-quantitative analysis of metabolism. Flies were initially fed with  $^{13}\text{C}_6$ -glucose, and the carbon-13 label was readily incorporated to primary metabolites. The yields of isotopic labeling of one target metabolite (uridine diphosphate glucose, UDP-Glc) were used as a proxy for the metabolic rates. The labeling – assessed based on the MALDI mass spectra – reflected the treatment applied to the fly stocks. A connection between circadian clock and the egg metabolism could be established. The study shows that a short-term perturbation to the day/night cycle has little effect on the metabolic rates in eggs – as assessed based on the labeling of UDP-Glc. In the second part of this work, we proposed a method for the analysis of sweat metabolites. The method combines facile sampling of sweat and detection by nanospray desorption electrospray ionization (nanoDESI)-MS. The samples were collected by using adhesive plasters as sampling tools, which was followed by nanoDESI-MS detection without any sample pretreatment. In this study, we implemented a home-made nanoDESI source, and tested it using standard compounds. Following a brief optimization of the detection method, the real samples were analyzed. In the resulting nanoDESI mass spectra, we could find peaks, which may correspond to sweat metabolites; however, a thorough identification of these putative metabolites has yet to be conducted. The main advantage of this method is its simplicity: sweat samples can be collected within a few seconds, and the analysis by nanoDESI-MS takes only several minutes.



## 開發質譜法偵測生物代謝體之方法及應用

學生：曾德璋

指導教授： 帕偉鄂本教授

陳月枝教授

國立交通大學應用化學系碩士班

### 摘 要

在此論文中，主要是以探討利用質譜法於果蠅卵子與人體汗水等生物檢體代謝物之分析與應用。在論文第一部份，我們藉由果蠅餵食具有穩定同位素碳十三葡萄糖發展活體同位素標定技術並以基質輔助雷射脫附游離質譜法維分析技術，進而取得果蠅的代謝體變化之訊息，自研究之結果中我們發現此方法可獲得果蠅單一卵子之半定量分析資訊。實驗中經餵食全碳十三葡萄糖的果蠅，碳十三同位素可進入果蠅的代謝過程中，在此我們將以目標代謝物—尿苷二磷酸的碳十三標定程度代表代謝速度，藉此標定程度我們發現此方法可反映環境變化對果蠅代謝速度的影響。在分析結果中，我們發現實驗組中調控短暫的日夜顛倒即可立即反應在果蠅卵子之代謝體，實驗組之果蠅卵子中的代謝體與控制組的果蠅卵子的標定程度結果幾乎一樣。而論文的第二部份，開發了一分析人體汗水代謝體之方法，藉由新穎之奈米噴灑脫附電噴灑游離質譜技術偵測以醫療膠布快速可收集來自於皮膚汗水樣品。此方法結合醫療膠布的快速取樣，不需任何前處理步驟即以奈米噴灑脫附電噴灑游離質譜分析。我們首先以自製的奈米噴灑脫附電噴灑游離源分析標準品，以確立此游離源之可行性，接著進行真實樣品汗液的分析，實驗中可以看到和背景梨子有差異的幾支離子峯，然而這些離子峯的確認還有待進一步的分析。並且我們將取樣及分析的過程做最佳化調整，此方法之優點在於可在幾秒鐘即可將樣品收集完成，且可在幾分鐘內完成質譜分析。

## Acknowledgement

首先要先感謝國科會與跨領域科學中心資助這項計畫，以及交通大學提供設備及儀器。感謝台大醫學院吳君泰老師的幫忙，果蠅實驗才得以順利完成。感謝帕偉鄂本教授及陳月枝教授的指導，讓我在碩士生涯可以學習到這麼多做人處事的道理。

終於來到這一刻，兩年來的點點滴滴要在這裡畫下句點。要把這些日子用文字表達出來實在不是那麼容易，不論是感謝或是經歷，都只能從文字上想像，但這條路要自己走過才知道，而才懂之前學長姐說的是甚麼，因為回首每一幕，都是自己留下的足跡，那是一條屬於自己的路，然而這裡的句點會留在這裡，在這裡學到最重要的是人要活在當下，並要繼續走出自己的康莊大道。

在這期間遇到了太多人，讀研究所與大學最大的差別就是每一天都面對同樣的幾個人，說在上班也不是在上班，說是上學又有錢拿，雖然很少，對此我想對在學期間遇到的人說聲謝謝，沒有你們就沒有現在的我。大叔、韓三、喳喳、采蓉、巴斯、張大哥，帶領我進入碩班的生活，李柏、大包、肉圓、達儒，是一同共患難的戰友，尤其是李柏，我想我說甚麼鳥事，他應該都懂，傑筆、小禿、書玄、煒茹，謝謝你們帶來的歡笑和娛樂，讓我可以開懷大笑，不爽的時候也可以跟你們抱怨，你們要撐住，就快解脫了，加油，丁煦、凱達你們最要撐住，因為選了這條路，一定不好走，但老師是不錯的，只要認真我相信一定可以有不錯的成果可以發表，其他雜事你們就要彼此分擔，加油!還有很多人很多事，如果真的要打完，大概要寫個十幾頁，不過我想你們會懂得。

最後我要畢業了，謝謝大家。

德瑋

# Table of Contents

## **CHAPTER 1: Introduction----- 1**

1.1 Analysis of metabolites in biological samples -----	1
1.2 Mass spectrometry -----	2
1.3 Ion sources used in this work -----	4
1.4 Time-of-flight mass analyzer -----	7
1.5 Ion trap mass analyzer -----	9
1.6 Goals of the work-----	11

## **CHAPTER 2: Isotope label-aided mass spectrometry reveals the influence of environmental factors on metabolism in single eggs of fruit fly--- 12**

2.1 Background-----	12
2.2 Experimental section-----	16
2.2.1 Fly stocks-----	16
2.2.2 Isotopic labelling -----	16
2.2.3 Dissection of flies and sample preparation -----	17
2.2.4 Mass spectrometry -----	17
2.2.5 Data treatment -----	18
2.3 Results and discussion-----	18
2.3.1 Preliminary experiments and optimization-----	18
2.3.2 Isotopic labelling of fruit flies-----	22
2.3.3 Time course of UDP-Glc labelling -----	25
2.3.4 Influence of the incubation conditions on the isotopic labelling of eggs -----	27
2.3.5 Influence of circadian adaptation on the labelling of eggs -----	28
2.3.6 Labelling variability -----	33
2.4 Concluding remarks-----	40

## **CHAPTER 3: Facile sampling of sweat combined with direct analysis of metabolites by nanoDESI-MS----- 41**

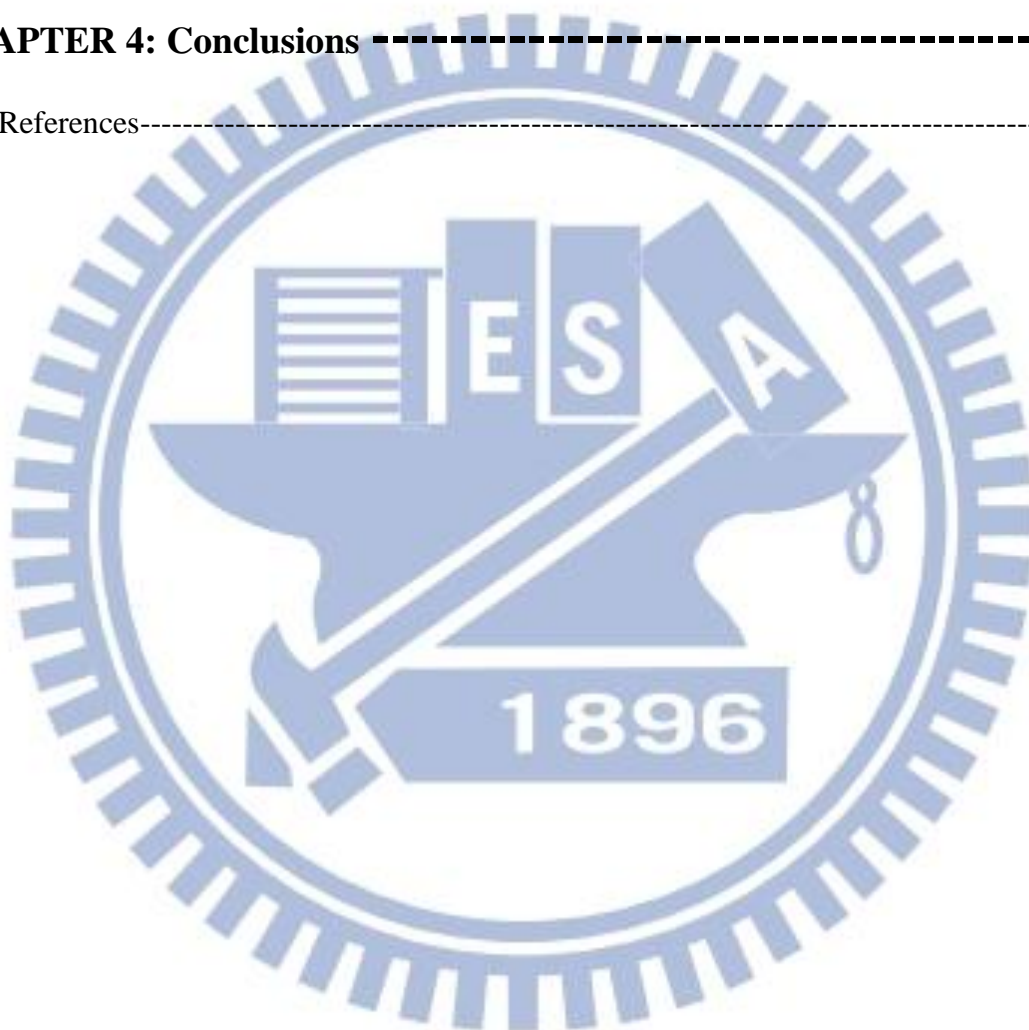
3.1 Background-----	41
3.2 Experimental section-----	44
3.2.1 Materials-----	44
3.2.2 Collecting real samples-----	44
3.2.3 Construction of the nanoDESI source-----	46
3.2.4 Mass spectrometry instrumentation -----	46
3.2.5 Data processing-----	47



3.3 Results and discussion	47
3.3.1 Setup of the nanoDESI-MS system	47
3.3.2 Testing the interface	48
3.3.3 Recording blank spectra of various solvent systems	50
3.3.4 Comparison of various sampling materials	51
3.3.5 Analysis of a sweat sample	56
3.3.6 Direct sampling of sweat from skin followed by nanoDESI-MS	58
3.3.7 The influence of sampling time	61
3.4 Concluding remarks	63

**CHAPTER 4: Conclusions** ----- **65**

References	67
------------	----



# List of Figures

- Figure 1.1.** General scheme of a mass spectrometer. Several types of sample inlets can be attached to the ion source housing. Transfer of the sample from atmospheric pressure to the high vacuum of the ion source and mass analyzer is accomplished by using of a vacuum lock. Figure reproduced from: J. H. Gross (2011) *Mass Spectrometry*. Springer, Berlin -----3
- Figure 1.2.** Schematic of the primary and secondary ionization processes in MALDI. The fat arrow represents the laser pulse, the gray circles represent the matrix, the dark hexagons represent the sample. (a) Within a few tens of nanoseconds of the laser pulse, initial charges are generated, mostly matrix and cations/anions from additives in the samples (e.g., cationization agents in the case of polymers). A phase of frequent collisions and charge transfer reactions in the dense plume follows. (b) Within a fraction of a microsecond after the laser pulse, the plume has spread, analyte ions have been charged by ion–molecule reactions in the plume, and, after several  $\mu\text{m}$  the dilution finally brings chemical reactions in the plume to a halt. The ions formed are extracted from the source region and detected. Figure reproduced from: L. Li. (2009) *MALDI : Mass Spectrometry for Synthetic Polymer Analysis..* Wiley, Hoboken-----5
- Figure 1.3.** Schematic of an early electrospray ion source design. Figure reproduced from: J. H. Gross (2011) *Mass Spectrometry*. Springer, Berlin -----6
- Figure 1.4.** Drawing of a decomposing droplet in an ESI source,  $q$  – charge;  $\epsilon_o$  – permittivity of the environment;  $\gamma$  – surface tension and  $D$  – diameter of a supposed spherical droplet. The sprayed direction of droplet is the same as the arrow pointing. Figure reproduced from: E. de Hoffmann, V. Stroobant (2001) *Mass Spectrometry. Principles and Applications*. Wiley, Hoboken -----6
- Figure 1.5.** Principle of a linear time-of-flight (TOF) instrument tuned to analyze positive ions produced by focusing a laser beam on the sample. Figure reproduced from: E. de Hoffmann, V. Stroobant (2001) *Mass Spectrometry. Principles and Applications*. Wiley, Hoboken-----7
- Figure 1.6.** Schematic representation of a TOF instrument equipped with a reflectron. Ions of a given mass have kinetic energy. The ions penetrate the reflectron until they reach zero kinetic energy and are then expelled from the reflector in opposite direction. The ion of bigger mass will reach the reflectron later, but come out with the same kinetic energy. The kinetic energy of the leaving ions remains unaffected, however their flight paths vary according to their differences in kinetic energy. Figure reproduced from: J. H. Gross (2011) *Mass Spectrometry*. Springer, Berlin. -----8
- Figure 1.7.** A time-of-flight (TOF) mass spectrometer fitted with a deflection electrode for precursor ion selection. The instrument can be operated in either linear or reflectron mode. Figure reproduced from: E. de Hoffmann, V. Stroobant (2001) *Mass Spectrometry. Principles and Applications*. Wiley, Hoboken.-----9



**Figure 1.8.** A quadrupole ion trap. (a) QIT with external ion source (illustration stretched in  $z$ -direction) and (b) section in the  $rz$ -plane. Figure reproduced from: J. H. Gross (2011) *Mass Spectrometry*. Springer, Berlin. ----- 10

**Figure 2.1.** Experimental design and chemical analysis workflow. (1) pre-conditioning (entrainment) of the culture stock (adaptation to the 12/12-h (light/dark) cycle); (2) incubation of female fruit flies with  $^{13}\text{C}_6$ -glucose solution; (3) dissection of the anesthetized flies; (4a/4b) preparation of individual eggs for mass spectrometric analysis; (5) mass spectrometry, and (6) data analysis.----- 15

**Figure 2.2.** Wide  $m/z$ -range negative-ion MALDI mass spectrum of a single egg obtained from fruit fly. Metabolites were extracted in situ using 50% acetonitrile solution. MALDI matrix: 9-aminoacridine. Labels of the most prominent peaks: ADP, adenosine diphosphate ( $m/z$  426); GDP, guanosine diphosphate ( $m/z$  442); ATP, adenosine triphosphate ( $m/z$  506); GTP, guanosine triphosphate ( $m/z$  522); UDP-Glc, uridine diphosphate glucose ( $m/z$  565); UDP-GlcNAc, uridine diphosphate *N*-acetyl glucosamine ( $m/z$  606).----- 19

**Figure 2.3.** Influence of the concentration of acetonitrile (ACN) in the extraction solution on the *signal-to-noise* ( $S/N$ ) ratios. This experiment included several metabolites (ATP,  $m/z$  506; GTP,  $m/z$  522; UDP-glucose,  $m/z$  565; and a phospholipid,  $m/z$  833) extracted from single eggs, and analyzed by MALDI-MS. ----- 21

**Figure 2.4.** Influence of the concentration of the 9-aminoacridine matrix solution (in acetone) on the *signal-to-noise* ( $S/N$ ) ratios of the peaks of various standard compounds. We found that at 6 mg mL<sup>-1</sup> 9-aminoacridine (in acetone), the  $S/N$  value is highest. Therefore, we chose this concentration of 9-aminoacridine for further experiments. -- 21

**Figure 2.5.** Isotopic labelling of ATP and UDP-Glc in single eggs. (A) MALDI mass spectra obtained from fruit flies following 1, 6, and 19 days of incubation with the  $^{13}\text{C}_6$ -glucose solution. (B) Reaction scheme of labelling glucose moiety in UDP-Glc with  $^{13}\text{C}_6$ -glucose.----- 23

**Figure 2.6.** MALDI-MS and MS/MS analysis of metabolites in the eggs of fruit flies incubated with  $^{13}\text{C}$ -glucose. Left: spectra for eggs obtained from flies incubated with  $^{12}\text{C}_6$ -glucose. Right: spectra for eggs obtained from flies incubated with  $^{13}\text{C}_6$ -glucose for 12 h. Evaluation of the MS/MS data was aided by the METLIN database (Scripps Center for Metabolomics, La Jolla, USA).----- 24

**Figure 2.7.** Progressive incorporation of the  $^{13}\text{C}$ -label to UDP-Glc in fruit fly eggs. The data points were fitted with a sigmoid function:  $y = 1.013 \cdot (1/(1+e^{(-0.135x+1.792)}))$ . During this experiment, the flies were incubated with  $^{13}\text{C}_6$ -glucose and illuminated with white light ( $\sim 4000$  lux). Note that the sampling intervals (as projected onto the  $x$ -axis) are coincidentally not constant. ----- 26

**Figure 2.8.** Influence of temperature (21 vs. 28 °C) and illumination (dark vs. light) on the labelling of glucose moiety in UDP-Glc molecules extracted from individual eggs. Female flies were incubated with  $^{13}\text{C}_6$ -glucose solution during 24 h. The default conditions were: white light on,  $\sim 4000$  lux (in the study involving the change of

temperature); temperature, 28 °C (in the study involving the change of illumination). 27

**Figure 2.9.** Histograms showing the distributions of labelling levels within the eggs obtained from the fruit flies incubated with  $^{13}\text{C}_6$ -glucose (during 12 h) at different illumination conditions and at different times during the day/night cycle. ML – flies incubated during day (starting from the morning) at light; MD – flies incubated during day (starting from the morning) at dark; EL – flies incubated during night (starting from the evening) at light; ED – flies incubated during night (starting from the evening) at dark. ----- 29

**Figure 2.10.** Histograms showing differences in the labelling of eggs among flies from the same treatment. Flies incubated during night (starting from the evening) at dark (ED): arbitrarily selected examples of five single-fly histograms, ordered according to the increasing level of labelling (Fly #1 to #5: top to bottom). All single-fly histograms from this experimental variant are displayed in **Figure 2.14**. ----- 34

**Figure 2.11.** Histograms showing differences in the labelling of eggs among flies from the same treatment (ML – flies incubated during day (starting from the morning) at light; black bars). Each of the small histograms (black bars) corresponds to a single fruit fly. The cumulative histogram for all the eggs obtained from the ML treatment (red bars). 36

**Figure 2.12.** Histograms showing differences in the labelling of eggs among flies from the same treatment (MD – flies incubated during day (starting from the morning) at dark; black bars). Each of the small histograms (black bars) corresponds to a single fruit fly. The cumulative histogram for all the eggs obtained from the MD treatment (red bars). 37

**Figure 2.13.** Histograms showing differences in the labelling of eggs among flies from the same treatment (EL – flies incubated during night (starting from the evening) at light; black bars). Each of the small histograms (black bars) corresponds to a single fruit fly. The cumulative histogram for all the eggs obtained from the EL treatment (red bars). 38

**Figure 2.14.** Histograms showing differences in the labelling of eggs among flies from the same treatment (ED – flies incubated during night (starting from the evening) at dark; black bars). Each of the small histograms (black bars) corresponds to a single fruit fly. The cumulative histogram for all the eggs obtained from the ED treatment (red bars). Selected histogram from this figure are also displayed in **Figure 2.10**. ----- 39

**Figure 3.1.** NanoDESI-MS setup used in this study. (a) 3D drawing of the setup (b) Photographs showing the assembly of the interface. Labels: (A) syringe, (B) grounding, (C) connector, (D) PEEK tubing, (E) sample stage, (F) one-axis stage, (G) XYZ-stage, (H) fitting, (I) connector, (J) fitting (K) solvent capillary, (L) plastic pipette tip, (M) solvent junction, (N) nanospray capillary, (O) MS inlet.----- 48

**Figure 3.2.** Testing the nanoDESI-MS setup with artificial samples. (a) Analysis of a dry 9-aminoacridine ( $m/z$  194) deposit on glass by nanoDESI-MS operated in the positive-ion mode. The sample was prepared in the following way: 2.0  $\mu\text{L}$  of  $10^{-4}$  M 9-aminoacridine solution in acetone were deposited on the tape, and dried. (b) Analysis of a dry creatinine ( $m/z$  113) deposit on glass by nanoDESI-MS operated in the positive-ion mode. The sample was prepared in the following way: 2.5  $\mu\text{L}$  of  $10^{-4}$  M creatinine solution in water were deposited on the glass, and dried. (c) Analysis of a dry



urea ( $m/z$  60) deposit on glass by nanoDESI-MS operated in the positive-ion mode. The sample was prepared in the following way: 2.0  $\mu\text{L}$  of  $10^{-4}$  M urea solution in water were deposited on the glass, and dried. The solvent mixture used in this nano-DESI experiment was composed of methanol and acetonitrile in the volume ratio 1:1, and it was spiked with acetic acid (final concentration,  $\sim 0.1\%$ ). ----- 49

**Figure 3.3.** A blank nano-DESI mass spectrum recorded in the negative-ion mode; no sample target was present in the solvent junction area. ----- 51

**Figure 3.4.** A positive-ion mode nano-DESI mass spectrum of plaster A (*cf.* **Table 3.1**). No sample has been deposited. The solvent mixture used in this nanoDESI experiment was composed of methanol and acetonitrile in the volume ratio 1:1, spiked with acetic acid (final concentration,  $\sim 0.1\%$ ). Several signals can be observed; for example, the peak at the  $m/z$  149 is most probably related to phthalic anhydride (molecular weight:  $148.1 \text{ g mol}^{-1}$ ), which is frequently used as plasticizer in consumer products. ----- 53

**Figure 3.5.** A blank nanoDESI mass spectrum recorded in the positive-ion mode; no sample target was present in the solvent junction area. The solvent used in this nanoDESI experiment was pure methanol (LC-MS grade). Comparison of different solvent systems used in nanoDESI experiments is presented in **Table 3.2**. ----- 54

**Figure 3.6.** Comparison of negative-ion mode nanoDESI mass spectra obtained for various materials tested in this study. No samples were spotted. The solvent used in this nanoDESI experiment was pure methanol (LC-MS grade). ----- 55

**Figure 3.7.** Analysis of a dry sweat deposit on plaster A by nanoDESI-MS operated in the positive-ion mode. Initially, the sweat sample was centrifuged at 8000 rpm for 20 min, and subsequently filtered using a 0.2- $\mu\text{m}$  syringe filter. The solvent mixture used in this nanoDESI-MS experiment was composed of methanol and acetonitrile in the volume ratio 1:1, spiked with acetic acid (final concentration,  $\sim 0.1\%$ ). ----- 56

**Figure 3.8.** Analysis of a dry sweat deposit on plaster A by nanoDESI-MS operated in the negative-ion mode. Initially, the sweat sample was centrifuged at 8000 rpm for 20 min, and subsequently filtered using a 0.2- $\mu\text{m}$  syringe filter. The solvent mixture used in this nanoDESI-MS experiment was composed of methanol and acetonitrile in the volume ratio 1:1, spiked with acetic acid (final concentration,  $\sim 0.1\%$ ). ----- 57

**Figure 3.9.** Analysis of a dry sweat collected directly on the plaster A by nanoDESI-MS operated in the positive-ion mode. The solvent mixture used in this nanoDESI-MS experiment was composed of methanol and acetonitrile in the volume ratio 1:1, spiked with acetic acid (final concentration,  $\sim 0.1\%$ ). ----- 59

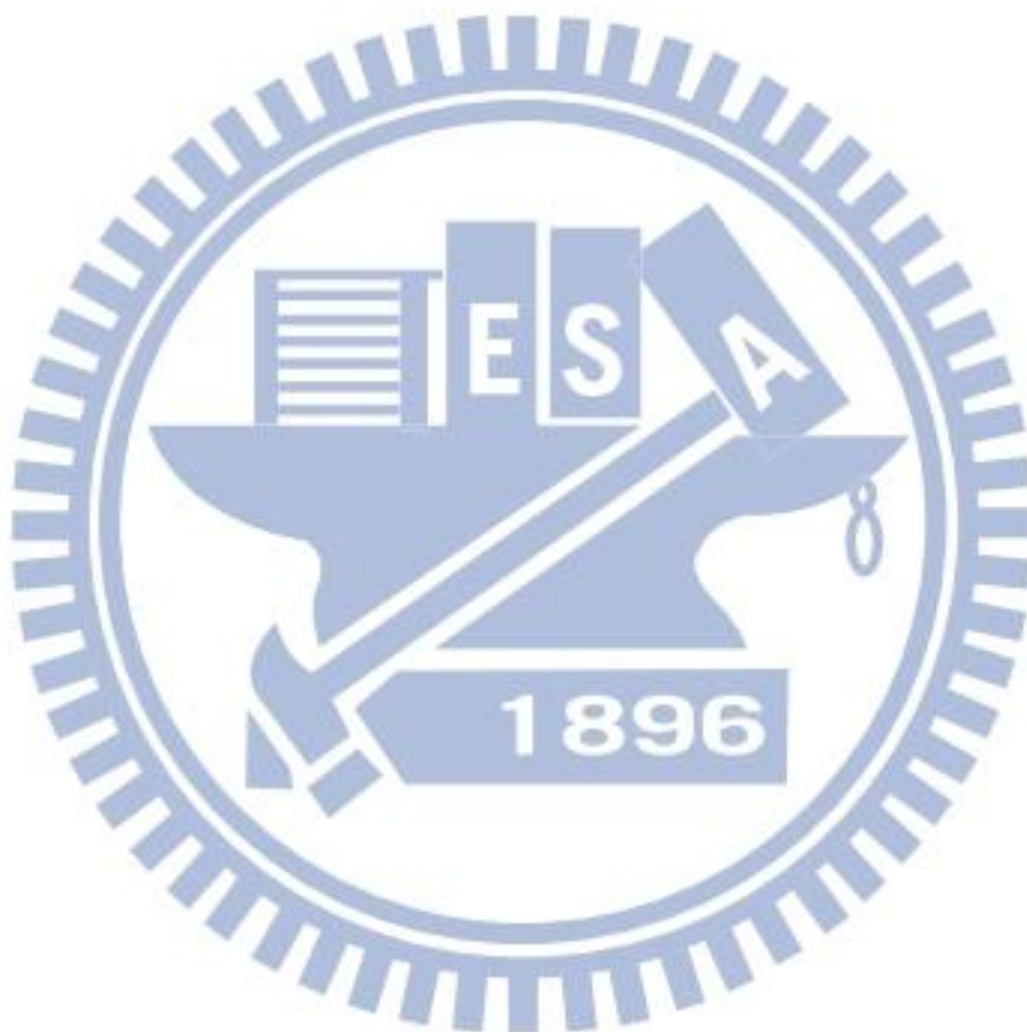
**Figure 3.10.** Analysis of a dry sweat collected directly on the plaster A by nanoDESI-MS operated in the negative-ion mode. The solvent mixture used in this nanoDESI-MS experiment was composed of methanol and acetonitrile in the volume ratio 1:1, spiked with acetic acid (final concentration,  $\sim 0.1\%$ ). ----- 60

**Figure 3.11.** Analysis of a sweat sample on plaster A, following incubation of the plaster with skin of a volunteer, using nanoDESI-MS operated in the negative-ion mode. The solvent



mixture used in this nanoDESI-MS experiment was pure methanol (LC-MS grade).-- 61

**Figure 3.12.** Analysis of a sweat sample on plaster A, following incubation of the plaster with skin of a volunteer, using nano-DESI-MS operated in the negative-ion mode. The sampling time was varied (1 – 300 s). The solvent mixture used in this nano-DESI experiment was composed of methanol and acetonitrile in the volume ratio 1:1, spiked with acetic acid (final concentration, ~ 0.1%). ----- 62



# List of Tables

<b>Table 2.1.</b> Statistical data on the samples analysed in this study. ML – flies incubated during day (starting from the morning) at light; MD – flies incubated during day (starting from the morning) at dark; EL – flies incubated during night (starting from the evening) at light; ED – flies incubated during night (starting from the evening) at dark.-----	30
<b>Table 2.2.</b> Results ( <i>p</i> -values) of the two-sample Kolmogorov-Smirnov test performed on the data obtained in this study. ML – flies incubated during day (starting from the morning) at light; MD – flies incubated during day (starting from the morning) at dark; EL – flies incubated during night (starting from the evening) at light; ED – flies incubated during night (starting from the evening) at dark. Null hypothesis: the two data sets are from the same continuous distribution. Red colour indicates the <i>p</i> -values where the null hypothesis is rejected (at the 5% significance level).-----	31
<b>Table 2.3.</b> Numbers of eggs with the labelling level higher or equal to 0.5 in each of the four groups. ML – flies incubated during day (starting from the morning) at light; MD – flies incubated during day (starting from the morning) at dark; EL – flies incubated during night (starting from the evening) at light; ED – flies incubated during night (starting from the evening) at dark.-----	31
<b>Table 3.1.</b> Features of the sampling materials used in this study.-----	45
<b>Table 3.2.</b> Performance of various solvent systems tested in this study. The quality of baseline and sensitivity were judged based on series of experiments with standards/real samples.-----	62

# List of Abbreviations

<b>9-AA</b>	9-Aminoacridine
<b>ACN</b>	Acetonitrile
<b>ATP</b>	Adenosine triphosphate
<b>CAPI</b>	Contactless Atmospheric Pressure Ionization
<b>DART</b>	Direct Analysis in Real Time
<b>DESI</b>	Desorption Electrospray Ionization
<b>EASI</b>	Easy Ambient Sonic-spray Ionization
<b>ED</b>	Flies incubated during night (starting from the evening) at dark
<b>EL</b>	Flies incubated during night (starting from the evening) at light
<b>ESI</b>	Electrospray Ionization
<b>GC</b>	Gas Chromatography
<b>Glc</b>	Glucose
<b>LC</b>	Liquid Chromatography
<i>m/z</i>	<i>Mass-to-charge</i> ratio
<b>MALDI</b>	Matrix-Assisted Laser Desorption/Ionization
<b>ML</b>	Flies incubated during day (starting from the morning) at light
<b>MD</b>	Flies incubated during day (starting from the morning) at dark
<b>MS</b>	Mass Spectrometry
<b>MS/MS</b>	“Tandem mass spectrometry”
<b>nano DESI</b>	Nanospray Desorption Electrospray Ionization
<b>SPME</b>	Solid-phase microextraction
<b>TOF</b>	Time-of-Flight (mass analyzer)
<b>UDP</b>	Uridine diphosphate
<b>UDP-Glc</b>	Uridine diphosphate glucose



# CHAPTER 1: Introduction

---

## 1.1 Analysis of metabolites in biological samples

Analysis of metabolites has had enormous importance in bioscience. It has led to important discoveries in biochemistry, and facilitated diagnosis of diseases. In the 21<sup>st</sup> century, the analysis of metabolites in biological samples is playing a key role in fundamental and applied research. Due to the improvements in analytical technology, one can nowadays obtain more comprehensive information about complex biological samples.

Every biological cell contains hundreds, if not thousands, of metabolites. In essence, metabolomics deals with identification, quantification of metabolites in biochemical network.<sup>1</sup> It investigates chemical processes including metabolites. In fact, metabolites can be analyzed in several ways, which encompass: (i) target analysis,<sup>2</sup> (ii) metabolic profiling,<sup>3,4</sup> and (iii) metabolomics.<sup>5,6,7</sup> The “target analysis” refers to quantitative analysis of metabolites.<sup>2</sup> Appropriate sample preparation can be performed in order to achieve a high sensitivity, and quantify less abundant metabolites. On the other hand, “metabolic profiling” is analysis of a class of compounds related to particular pathways.<sup>4</sup> In fact, the metabolic profiling approaches the final goal of an “unbiased metabolomics”.<sup>5,6,7</sup> However, this goal is very hard to achieve. Nielsen *et al.*<sup>8</sup> introduced the term of endo- and exo-metabolome to distinguish intra- and extra-cellular metabolites. According to this publication, metabolic fingerprinting is a semi-quantitative analysis of endo-metabolome,<sup>9</sup> and the metabolic

footprinting is a semi-quantitative analysis of the exo-metabolome.<sup>10</sup> Metabolic fingerprinting and metabolic footprinting are complementary to metabolic profiling.

There exist a variety of analytical techniques, which can be applied to study metabolites. Various instruments can also be combined (hyphenated) to provide high-performance analytical platforms. Direct-infusion mass spectrometry (MS), as well as chromatography coupled with MS are very useful techniques, which can fulfill some of the requirements of metabolite analysis.<sup>11,12</sup> One advantage of using mass spectrometry is its ability to distinguish between different isotopes.<sup>13,14</sup> In this way, one can label metabolites *in vivo*, and study biosynthetic pathways. Carbon-13 is one of the most frequently used isotopes in such experiments. This approach is frequently used in conjunction with chemical analysis by liquid chromatography (LC) coupled with MS. The following paragraphs outline the main ideas behind mass spectrometry – the analytical technique which has been chosen for this project.

## 1.2 Mass spectrometry

In general, the purpose of mass spectrometry is to measure mass-to-charge ( $m/z$ ) ratios of charged particles. Since many molecules and microscale particles are electrically charged (or can easily acquire electric charge), mass spectrometry is relevant to various disciplines of science, including physics, chemistry, and biology. In 1897, Dr Joseph John Thomson discovered electron, and determined its  $m/z$  ratio; since then, enormous developments have been made in the area of mass spectrometry. The basic components of mass spectrometers are: (1) ion source; (2) mass analyzer; (3) detector (**Figure 1.1**).

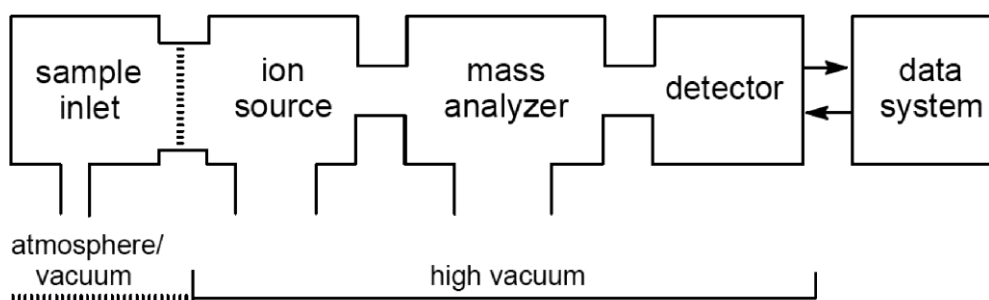


**Figure 1.1.** General scheme of a mass spectrometer. Several types of sample inlets can be attached to the ion source housing. Transfer of the sample from atmospheric pressure to the high vacuum of the ion source and mass analyzer is accomplished by using of a vacuum lock. Figure reproduced from: J. H. Gross (2011) *Mass Spectrometry*. Springer, Berlin

In the course of mass spectrometry, analytes must be converted into gas-phase ions. Subsequently, the mass analyzer – the heart of every mass spectrometer – separates the ions by mass-to-charge ( $m/z$ ) ratio. Eventually, the detector collects the separated ions, and sends out electrical signals. Except some ion sources, these processes take place under high vacuum, so the possible collisions of ions with other gas-phase molecules are reduced to minimum. Nowadays there are several commonly used MS techniques, including gas chromatography mass spectrometry (GC-MS), liquid chromatography mass spectrometry (LC-MS), direct infusion electrospray ionization mass spectrometry (ESI-MS), matrix-assisted laser desorption/ionization mass spectrometry (MALDI-MS), Fourier transform mass spectrometry (FT-MS), and inductively coupled plasma mass spectrometry (ICP-MS). Overall, mass spectrometry is a versatile technique which permits analysis of a huge variety of samples and chemical compounds. Over one century, significant progress has been made in this field, including the developments in all the three stages of the MS process described above. In the experimental work described in this thesis, which focuses on the analysis of metabolites, we used matrix-assisted laser desorption/ionization time-of-flight (TOF) mass spectrometry as well as nanospray desorption electrospray ionization (nanoDESI) ion trap (IT) mass



spectrometry. In the following paragraphs we will introduce the common ion sources (ESI and MALDI), as well as two mass analyzers (TOF and IT) used in this study.

### 1.3 Ion sources used in this work

In this work, we adopted two MS-based methods, one involving MALDI-MS, and the other one involving atmospheric pressure MS.

The MALDI source was introduced by Hillenkamp *et al.*<sup>15</sup> It is usually coupled with time-of-flight analyzers (see section 1.4). Desorption and ionization of analytes co-crystallized with a matrix occurs when ultraviolet (UV) pulsed laser light impinges on the sample deposit (**Figure 1.2**). MALDI matrices are normally small organic molecules which can readily co-crystallize with the analyte. Matrix molecules also need to absorb UV light and transform to excited state. Due to the large amount of heat in the matrix and the sample are vaporized.<sup>16</sup> Some reports suggest the excited-state proton transfer<sup>16</sup> may facilitate ionization of the analyte.<sup>17</sup> However, the ionization mechanism involved in the MALDI process is still not clear. The matrices, such as  $\alpha$ -cyano-4-hydroxycinnamic acid (CHCA), sinapinic acid (SA) and trihydroxyacetophenone monohydrate (THAP) are fluorescent, which suggests the importance of transferring the energy from laser light onto analyte molecules. Advantages of MALDI-MS are: simple sample preparation, formation of singly charged ions, and high sensitivity. MALDI also has some drawbacks: the crystallization of matrix/sample deposits is usually non-homogeneous. This leads to poor repeatability and moderate quantitative capabilities. Matrix ions usually give rise to high interference in the low- $m/z$  range, in particular below 500.

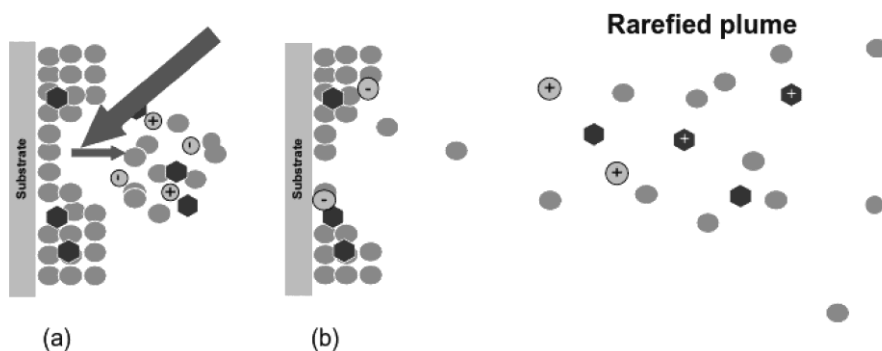


**Figure 1.2.** Schematic of the primary and secondary ionization processes in MALDI. The fat arrow represents the laser pulse, the gray circles represent the matrix, the dark hexagons represent the sample. (a) Within a few tens of nanoseconds of the laser pulse, initial charges are generated, mostly matrix and cations/anions from additives in the samples (*e.g.*, cationization agents in the case of polymers). A phase of frequent collisions and charge transfer reactions in the dense plume follows. (b) Within a fraction of a microsecond after the laser pulse, the plume has spread, analyte ions have been charged by ion-molecule reactions in the plume, and, after several  $\mu\text{m}$  the dilution finally brings chemical reactions in the plume to a halt. The ions formed are extracted from the source region and detected. Figure reproduced from: L. Li. (2009) *MALDI : Mass Spectrometry for Synthetic Polymer Analysis.* Wiley, Hoboken

The electrospray ionization (ESI) technique for MS was introduced by Fenn *et al.*,<sup>18</sup> and it soon showed to be very useful in the mass spectrometric analysis of biomolecules, including proteins. In ESI, the ionization process is normally accomplished under atmospheric pressure. Electrospray is produced by applying a strong electric field to a liquid transfer capillary under atmospheric pressure (**Figure 1.3**). The so-called “Taylor cone” is formed at the outlet of the capillary, and small liquid droplets detach and fly towards the counter-electrode. The breakdown of charged droplets into smaller droplets can be explained with the Rayleigh principle (**Figure 1.4**): when the charged droplets are formed of the Taylor cone, the solvent of charged droplet is evaporated by the heated drying gas, which enhances the repulsion between electric charges, and contributes to breaking down the droplets into

smaller droplets. The analyte species is often acquire multiple charges in this process. Clearly, the mechanism of ESI is very different than that of MALDI; unlike MALDI, ESI gives rise to multiply charged ions ( $z > 1$ ). In consequence, large molecules can be analyzed on mass analyzers with relatively narrow  $m/z$  range.

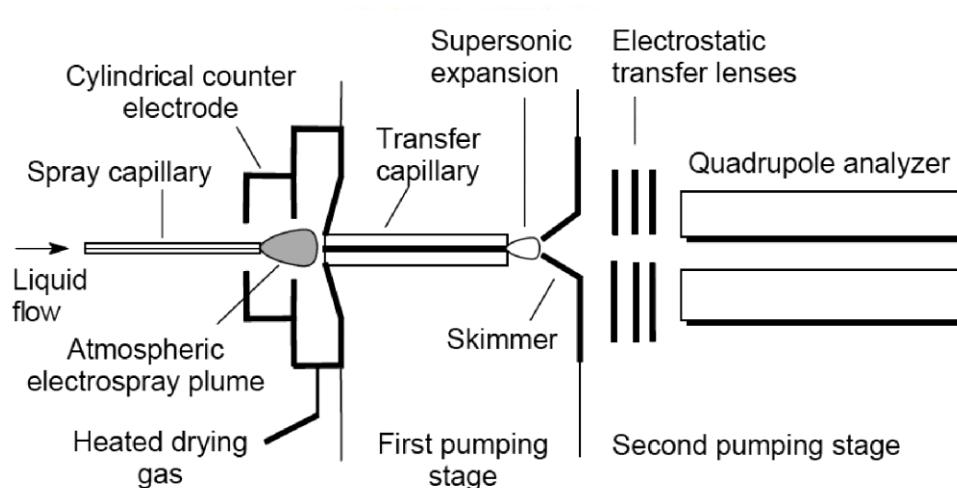


**Figure 1.3.** Schematic of an early electrospray ion source design. Figure reproduced from: J. H. Gross (2011) *Mass Spectrometry*. Springer, Berlin

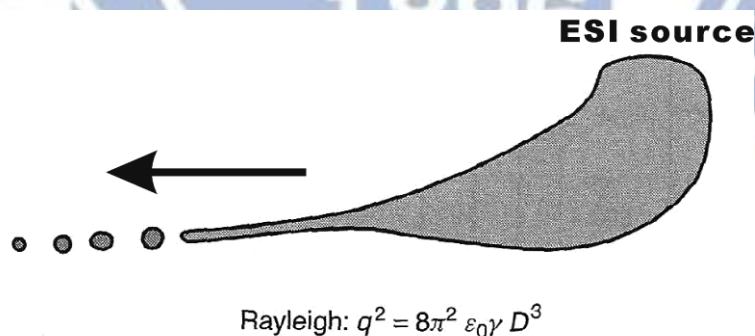


**Figure 1.4.** Drawing of a decomposing droplet in an ESI source,  $q$  – charge;  $\epsilon_o$  – permittivity of the environment;  $\gamma$  – surface tension and  $D$  – diameter of a supposed spherical droplet. The sprayed direction of droplet is the same as the arrow pointing. Figure reproduced from: E. de Hoffmann, V. Stroobant (2001) *Mass Spectrometry. Principles and Applications*. Wiley, Hoboken



## 1.4 Time-of-flight mass analyzer

The time-of-flight analyzer measures the time elapsed from when ions are expelled from the ion source (and accelerated by a potential  $V_s$ ) till they reach the detector (**Figure 1.5**).<sup>19,20</sup>

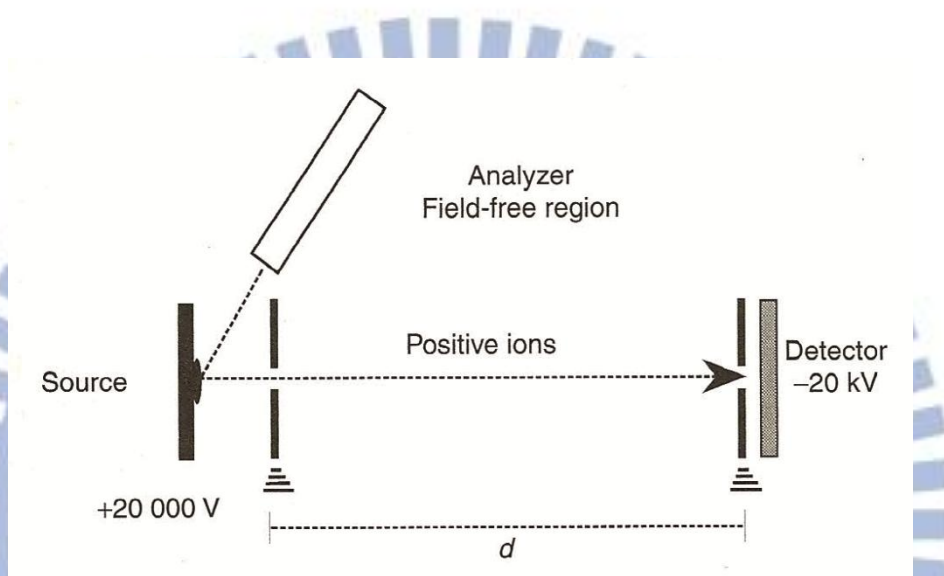


**Figure 1.5.** Principle of a linear time-of-flight (TOF) instrument tuned to analyze positive ions produced by focusing a laser beam on the sample. Figure reproduced from: E. de Hoffmann, V. Stroobant (2001) *Mass Spectrometry. Principles and Applications*. Wiley, Hoboken

The distance between the source and the detector is denoted by  $d$ . An ion with mass  $m$  and a total charge  $q = ze$  ( $e$  is the electric charge of  $-1.602 \times 10^{-19}$  coulomb) has the kinetic energy:  $qV_s$ . The flight time of an ion is denoted as  $t$ . We can measure  $t^2$  and determine the value of mass-to-charge ( $m/z$ ) ratio according to the following equation:

$$\frac{m}{z} = t^2 \left( \frac{2V_s e}{d^2} \right)$$

The mass resolution depends on the length of the TOF tube. Using long TOF tubes increases the cost, and increases the overall size of the device. However, mass resolution can

also be increased in a different way, without extending the length of the TOF tube. TOF analyzers usually feature an electrostatic reflector called “reflectron” (**Figure 1.6**).

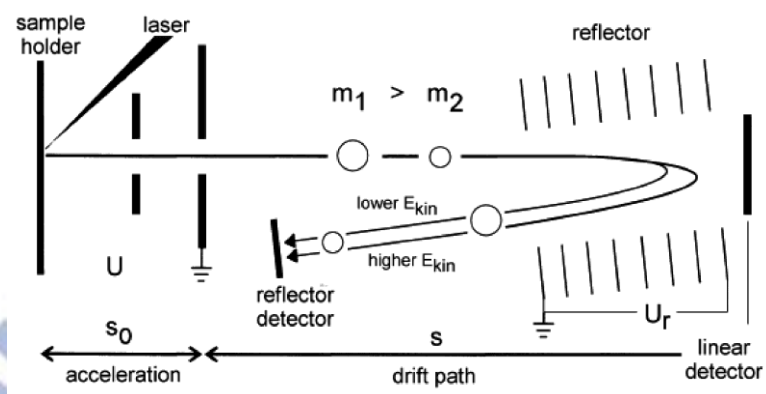


**Figure 1.6.** Schematic representation of a TOF instrument equipped with a reflectron. Ions of a given mass have kinetic energy. The ions penetrate the reflectron until they reach zero kinetic energy and are then expelled from the reflectron in opposite direction. The ion of bigger mass will reach the reflectron later, but come out with the same kinetic energy. The kinetic energy of the leaving ions remains unaffected, however their flight paths vary according to their differences in kinetic energy. Figure reproduced from: J. H. Gross (2011) *Mass Spectrometry*. Springer, Berlin.

Reflectron consists of several ring electrodes positioned at the end of the flight tube. A voltage of polarity that is opposite to the charge of the ions is applied to these electrodes. When ions enter the reflectron area, they are reflected, and they migrate to a detector positioned close to the center of the TOF tube. This way, the time of flight increases. The ions with greater kinetic energy enter a deeper section within the reflectron cavity, as compared with the ions which have carried less kinetic energy. As a result, the mass resolution increases. Two TOF sections can be put together in order to enable “tandem-in-space” mass spectrometry. Fragmentation of precursor ions, which reach the fragmentation cell, can be realized by collision-induced dissociation (CID) or post-source decay (PSD). The fragments are subsequently separated in the TOF tube and reach the detector (**Figure 1.7**). The

instrument is operated by a co-linear arrangement of two TOF mass analyzers, each equipped with an ion source that allows acceleration and focusing of the ions. In TOF1, the analyte ions are accelerated, precursor ions are selected and fragmented. Fragment ions are allowed to proceed to the “source” of TOF2, where they are accelerated and analyzed.<sup>21</sup>

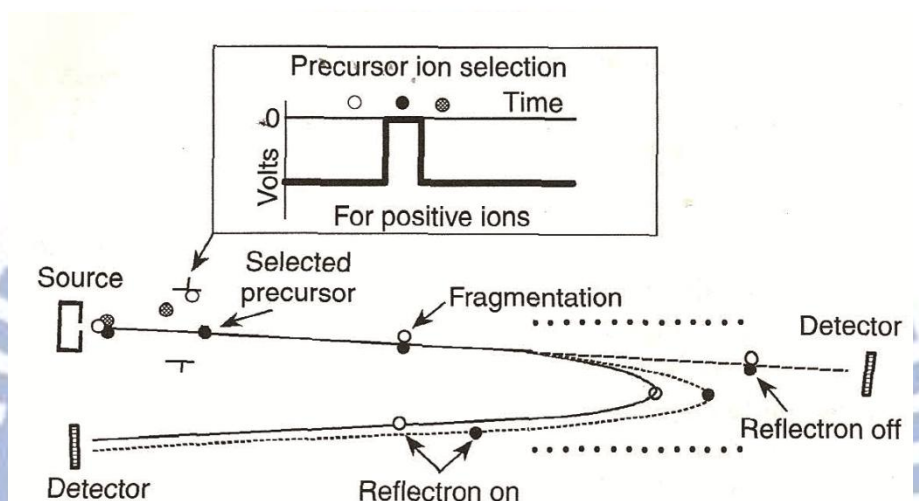


**Figure 1.7.** A time-of-flight (TOF) mass spectrometer fitted with a deflection electrode for precursor ion selection. The instrument can be operated in either linear or reflectron mode. Figure reproduced from: E. de Hoffmann, V. Stroobant (2001) *Mass Spectrometry. Principles and Applications*. Wiley, Hoboken.

## 1.5 Ion trap mass analyzer

The ion trap mass analyzer consists of an upper and a lower cap mounted on both sides of a ring electrode. The motion of ions in ion trap can be explained by the Mathieu equation.<sup>22,23</sup> The motion of ions in a three-dimensional space is influenced by the potentials applied to the electrodes. For an ion to stay in the ion trap it must have a stable ion motion along both  $z$  and  $r$ . An additional resonant AC voltage which has the the same frequency of oscillating ions in  $z$  direction is applied, and the trapped ions are oscillated until their trajectories are destabilized, and the ions are ejected from the trap in the  $z$  direction.



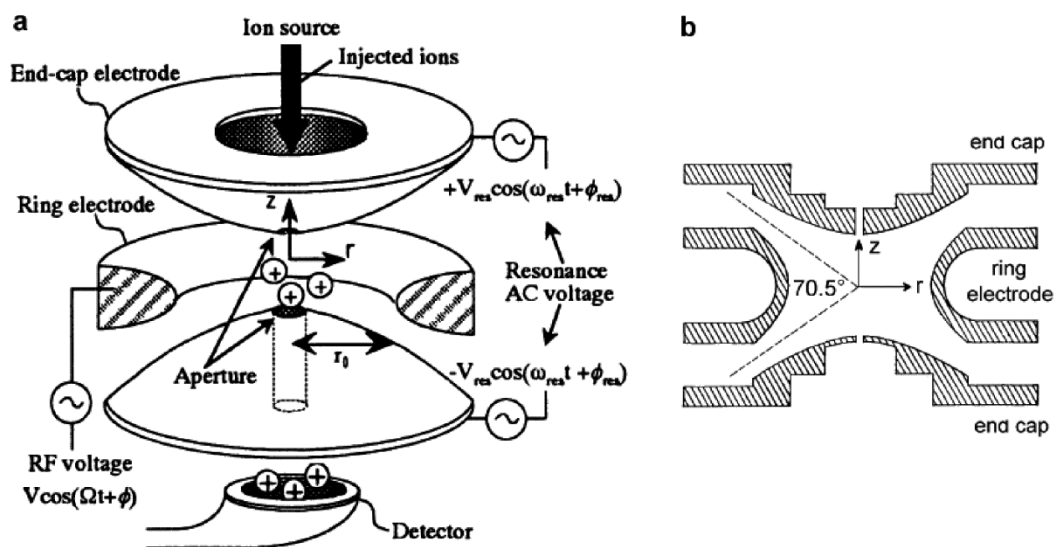


**Figure 1.8.** A quadrupole ion trap. (a) QIT with external ion source (illustration stretched in  $z$ -direction) and (b) section in the  $rz$ -plane. Figure reproduced from: J. H. Gross (2011) *Mass Spectrometry*. Springer, Berlin.

Ion trap also enables tandem MS analysis. Contrary to the TOF/TOF instruments, the MS/MS analysis in the ion trap can be described as “tandem-in-time” because it takes place in one mass analyzer. As it can be deduced from stable region ions can be selected by adjusting the values of  $U$  (DC voltage) and  $V$  (RF voltage). Therefore, the ions with a given  $m/z$  ratio can be trapped, and used as parent ions during the fragmentation step. A higher resonant voltage ( $V$ ) is applied on the ring electrode to increase oscillating energy to carry out the fragmentation. Eventually,  $m/z$  values of the fragment ions can be recorded by sweeping the amplitude of RF voltage which is applied on the end-cap electrode.

## 1.6 Goals of the work

In this study, we aim to develop mass spectrometric methods facilitating the analysis of metabolites in different kinds of biological samples: (i) single eggs of fruit fly, and (ii) human sweat. In the following chapters, we provide information about the experiments conducted, and discuss technical obstacles that had to be overcome.

In order to measure metabolic rates in microscale samples obtained from individual fruit flies, we use MALDI-MS. However, MALDI-MS has poor quantitative capabilities. To solve this problem, we aimed to implement *in-vivo* labelling of fruit flies with  $^{13}\text{C}$ -labelled glucose, followed by subsequent monitoring of the labelling yields of a selected target metabolite by mass spectrometry.

In another study, in order to detect metabolites secreted by skin with sweat, we propose strategy which combines passive sampling with direct mass spectrometric analysis. This method should does not require any sample pretreatment. Since sweat samples are generally hard to collect and analyze by conventional analytical tools, we believe that setting up this method will open new possibilities for clinical analysis and doping control.

# CHAPTER 2:

## Isotope label-aided mass spectrometry reveals the influence of environmental factors on metabolism in single eggs of fruit fly

---

### 2.1 Background

Circadian clock helps biological organisms to control their physiological and developmental processes.<sup>24</sup> Biological rhythmicity is common in nature, with environmental factors – such as light and temperature – synchronizing internal time of the organisms to the 24-h cycle.<sup>25</sup> Although daily rhythms are often measured as activity vs. rest, other parameters – including the level of behaviour or gene expression – are also changing with a circadian period.<sup>25</sup> In humans, any disruption to the circadian rhythm can affect physical and mental performance. For example, insomnia is a common problem known to many travelers who experience jet lag.<sup>26</sup> Disruption of circadian rhythms can also lead to metabolic disorders.<sup>27</sup> Thus, studying relationships between circadian rhythms and metabolism may contribute to a better understanding of the mechanism and robustness of the biological clock. So far, most concepts in molecular regulation of circadian rhythms in eukaryotic cells have been based on transcription-translation feedback loops; however, a recent study demonstrated the existence

of a phenotypic circadian clock in red blood cells – *i.e.* in a biological system where no transcription occurs.<sup>28</sup>

Small metazoa are convenient models for studying circadian rhythms; one of them is fruit fly (*Drosophila melanogaster*).<sup>29</sup> In fact, fruit fly is the most studied invertebrate, and a large amount of scientific information about this species is currently available.<sup>30,31</sup> Although fruit fly has served as a model organism in several studies of circadian rhythms,<sup>32,33,34</sup> limited data is currently available on the influence of circadian adaptation of fruit fly on primary metabolism in this species. The small volumes of samples obtained from individual flies disable the possibility of analyzing relevant metabolites using conventional analytical tools.

There exist a number of analytical techniques applicable to the analysis of metabolites in biological samples; two prominent examples include the coupling of liquid chromatography, or gas chromatography with mass spectrometry. The GC-MS platform enables analysis of volatile analytes in large numbers of samples; it offers high sensitivity, reproducibility, and can easily be automated.<sup>3</sup> Implementation of chromatographic techniques usually necessitates pre-treatment of the samples. In most cases, this renders LC-MS and GC-MS inadequate to analysis of samples smaller than ~ 1 mm. In the past few years, matrix-assisted laser desorption/ionization<sup>15</sup> mass spectrometry has emerged as an enabling tool for the metabolic profiling of microscale samples;<sup>35,36</sup> it provides what the other analytical tools cannot offer: compatibility with micrometer-scale samples, high sensitivity, and it does not require complicated sample preparation. MALDI-MS takes advantage of laser beam to volatilize and ionize compounds embedded in a chemical matrix.<sup>37</sup> The matrix molecules absorb energy from the laser light, and transfer it onto the analyte molecules, which become ionized in the gas phase. A mass spectrum can be obtained right after a few shots of laser light impinge on a sample/matrix deposit. A major disadvantage of MALDI-MS is its



limited quantitative capability – a characteristic attributed to the limitations of sample preparation protocols, and ion suppression effects. When using MALDI-MS in the studies of metabolism, one possible solution to this problem is the implementation of stable-isotope labels.<sup>38,39</sup> The *in-vivo* labelling of fruit flies with stable isotopes – in combination with LC-MS – has already gained an insight into the proteome of fruit fly.<sup>40</sup> Therefore, to mitigate the problems related to the signal variability in MALDI-MS, here we have also implemented *in-vivo* isotopic labelling of metabolites in fruit flies.

In order to investigate the influence of circadian adaptation on egg metabolism, we have implemented the following protocol (**Figure 2.1**): First, fruit flies (*D. melanogaster*) are adapted to the day/night cycle using artificial white light. Second, female flies are incubated with <sup>13</sup>C-labeled glucose (the only carbon source) for 12 h – either during the circadian day or circadian night, either at light or at dark. The labelled carbohydrate is ingested by the flies, and metabolized. Third, samples of eggs are obtained from the incubated flies, and the relative abundances of metabolite isotopologues present in individual eggs are determined by MALDI-MS. We sought answers to the following questions: (i) Will <sup>13</sup>C-labelled glucose be used as a carbon source in primary metabolism, and will the <sup>13</sup>C atoms be incorporated into metabolites in individual eggs? (ii) Can MALDI-MS provide useful quasi-quantitative results (*i.e.* without performing absolute quantification), which would reflect the treatment applied to the fly stocks (*e.g.* variation of temperature or light)? (iii) Does the circadian clock affect metabolite labelling in female fruit flies?

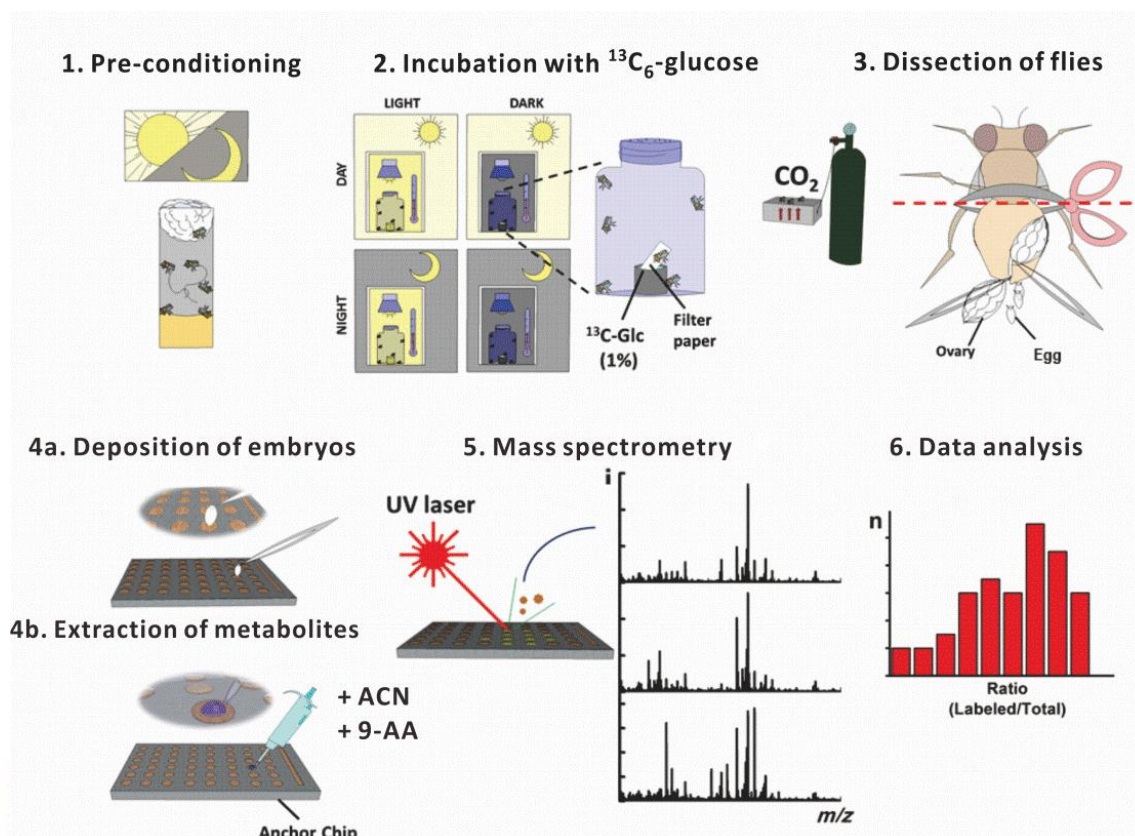


**Figure 2.1.** Experimental design and chemical analysis workflow. (1) pre-conditioning (entrainment) of the culture stock (adaptation to the 12/12-h (light/dark) cycle); (2) incubation of female fruit flies with  $^{13}\text{C}_6$ -glucose solution; (3) dissection of the anesthetized flies; (4a/4b) preparation of individual eggs for mass spectrometric analysis; (5) mass spectrometry, and (6) data analysis.

We have opted for measuring metabolite levels in the samples composed of single eggs. This choice was made due to several reasons: (i) Eggs can be considered as a sink for the absorbed nutrients and primary metabolites. (ii) Eggs occupy substantial volume in the fly abdomen, and the amount of the biological material contained in single egg is sufficient for the analysis by MALDI-MS. (iii) It is relatively easy to obtain multiple eggs from individual flies through manual dissection. (iv) Eggs are more compact, less vulnerable to osmolarity changes and mechanical stress, as compared with other fruit fly organs (*e.g.* ovarioles, gut, brain) which can be sampled for chemical analysis. Fruit fly eggs measure approximately half

millimeter, which can be regarded as an adequate size of a sample for the analysis by MALDI-MS following careful sample preparation.

## 2.2 Experimental section

### 2.2.1 Fly stocks

Fruit flies (*Drosophila melanogaster*;  $w^{1118}$  – a normal control strain purchased from the *Drosophila* Stock Center in the Department of Biology at Indiana University, USA) were reared on a standard medium (water, yeast, soy flour, yellow cornmeal, agar, light corn syrup, propionic acid) loaded into plastic vials. Typically, the stock culture was maintained at room temperature. The default photoperiod was 16-hr day / 8-hr night; however, during the entrainment period (before the experiments related to the circadian rhythms), it was changed to 12-hr day / 12-hr night.

### 2.2.2 Isotopic labelling

Female and male fruit flies were separated under stereomicroscope (Zeiss, Munich, Germany), and the female individuals were subsequently transferred into 100-mL glass vials (Richiden-Rika Glass Company, Kobe City, Japan). A plastic cap with a stripe of filter paper wetted with 1%  $^{13}\text{C}_6$ -glucose solution in water was inserted to each of the vials, so that the flies were exposed to the  $^{13}\text{C}_6$ -labelled glucose during the following hours/days. In most experiments, the vials were put inside an incubator in order to control the temperature. Most flies survived at least 7 days under these conditions. During the labelling experiments, illumination was provided by a light-emitting diode (LED) lamp (white light; Aliiv, Taipei, Taiwan), which ensured the illuminance of ~4000 lux. During the entrainment period, weaker



light (~ 150 lux) was used.

### **2.2.3 Dissection of flies and sample preparation**

Before the dissection, flies were anesthetized with carbon dioxide gas. Heads and abdomens were separated from thoraxes using miniature scissors (Vannas-Tübingen Spring; FST, Foster City, California). A set of precise tweezers (Dumont, Munich, Germany) was used to remove ovaries, and obtain unfertilized eggs (for a reference to the dissection protocol, see, for example: ref. 41). After brief washing in phosphate buffered saline solution, the eggs were transferred – one-by-one – onto separate recipient sites (i.d. 0.4  $\mu\text{m}$ ) of a metal AnchorChip plate (Bruker Daltonics, Bremen, Germany). Following the deposition of the eggs onto the target plate, an aliquot of 0.5  $\mu\text{L}$  1:1 (v/v) acetonitrile/water solution (after initial optimization) was pipetted to initiate extraction of metabolites from the egg; then, a 0.5- $\mu\text{L}$  aliquot of 6 mg  $\text{mL}^{-1}$  9-aminoacridine (Sigma-Aldrich, St Louis, USA; MALDI matrix) solution in acetone (Merck, Darmstadt, Germany) was added. Following the evaporation of the solvents, the resulting sample/matrix deposits were ready for analysis by mass spectrometry. Note that 9-aminoacridine is a carcinogen, and personal safety equipment must be used when handling preparations of this compound. Animal tissue residues are disposed off as biological waste.

### **2.2.4 Mass spectrometry**

During the mass spectrometric analysis, we used the AutoFlex III MALDI-time-of-flight (TOF)-MS from Bruker Daltonics, which is equipped with a solid-state laser ( $\lambda = 355 \text{ nm}$ ). Negative-ion mode was used with the following settings: ion source 1, -19.0 kV; ion source 2, -16.6 kV; lens, -8.45 kV; delay time, 0 ns. The



Smartbeam-laser focus was set to “small” (~40  $\mu\text{m}$ ); 100 shots were fired at each sample spot with the preset frequency of 50 Hz. The mass range was set to 400-1000 Da, and the suppression threshold was set to 400 Da, so that the low- $m/z$  ions (including the matrix ions) could not reach the detector.

## 2.2.5 Data treatment

The MS data were acquired using the FlexControl software (version 3.0; Bruker Daltonics), and further analyzed with the FlexAnalysis software (version 3.0; Bruker Daltonics). The output data were further used to calculate the ratios of peak areas at the  $m/z$ : 571/(565+571). These ratio values were used to plot histograms with the bin width of 0.1. Statistical analysis (one- and two-sample Kolmogorov-Smirnov test, Wilcoxon rank sum test) was conducted using the MATLAB software (version 7.6.0.324 (R2008a), MathWorks, Natick, USA). Curve fitting was conducted using the SPSS software (version 19, IBM Corp., New York, USA). Other data were treated and displayed using the Origin Pro software (version 8; Origin Lab Corporation, Northampton, USA).

## 2.3 Results and discussion

### 2.3.1 Preliminary experiments and optimization

Implementation of the proposed analytical workflow (**Figure 2.1**) has been preceded by a series of preliminary experiments. Initially, the *in-situ* extraction of metabolites from samples was tested and optimized. Metabolites were passively extracted from eggs on the MALDI target (AnchorChip, Bruker Daltonics), and co-crystallized with the matrix compound (9-aminoacridine). We chose to use acetonitrile as the extraction solvent since it has

widely been used for extraction of cellular metabolites (*e.g.* ref. <sup>42</sup>). During the optimization step, we tested mixtures of acetonitrile with water at different volume ratios. 9-Aminoacridine is a suitable matrix for MALDI-MS analysis of metabolites in the negative-ion mode.<sup>43</sup> Signals corresponding to several primary metabolites – which leaked out of the egg – could readily be identified in the MALDI mass spectra (*e.g.* **Figure 2.2**).

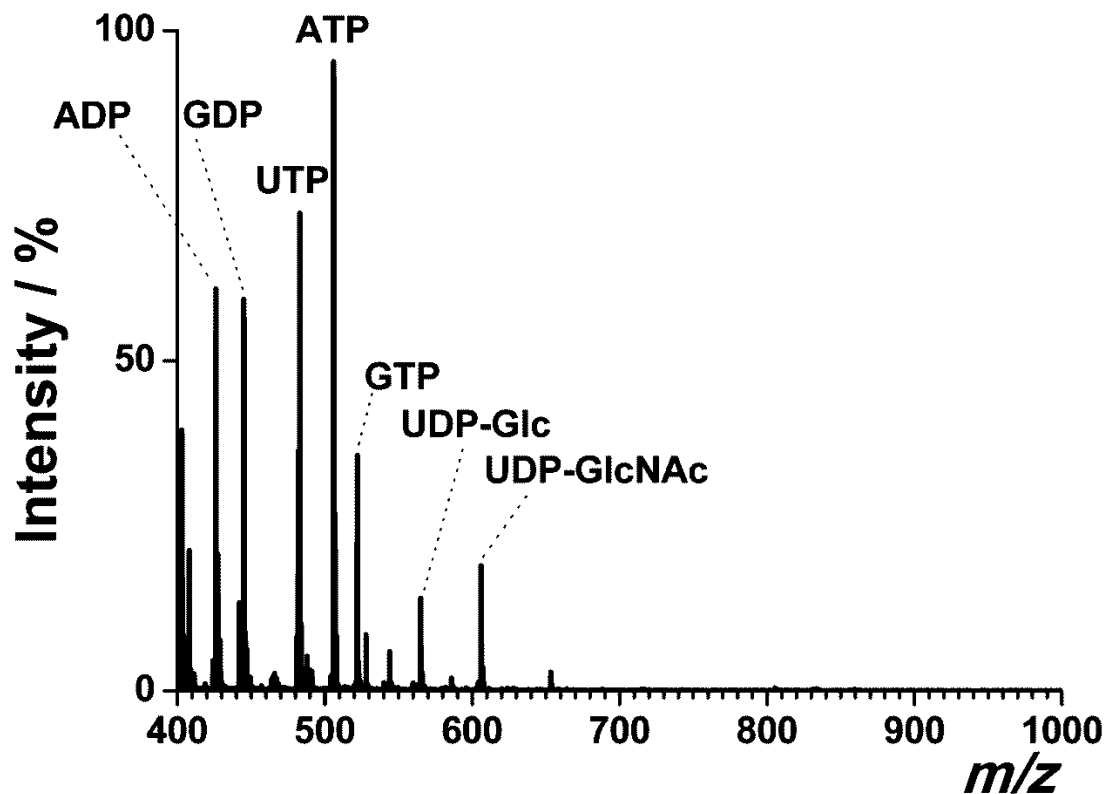


**Figure 2.2.** Wide  $m/z$ -range negative-ion MALDI mass spectrum of a single egg obtained from fruit fly.

Metabolites were extracted in situ using 50% acetonitrile solution. MALDI matrix: 9-aminoacridine. Labels of the most prominent peaks: ADP, adenosine diphosphate ( $m/z$  426); GDP, guanosine diphosphate ( $m/z$  442); ATP, adenosine triphosphate ( $m/z$  506); GTP, guanosine triphosphate ( $m/z$  522); UDP-Glc, uridine diphosphate glucose ( $m/z$  565); UDP-GlcNAc, uridine diphosphate *N*-acetyl glucosamine ( $m/z$  606).

The optimization of the sample preparation involved experiments in which the percentage of acetonitrile in the extraction solution as well as the concentration of 9-aminoacridine in the matrix cocktail were varied. Based on the measurements of signal-to-noise ( $S/N$ ) ratios in the resulting spectra (**Figures 2.3** and **2.4**), we chose acetonitrile mixed with water at the ratio 1:1 (v/v) as the extraction solvent, and  $6 \text{ mg mL}^{-1}$  9-aminoacridine solution in acetone as the MALDI matrix cocktail. It is believed that at low percentage of acetonitrile, biological membranes are not destabilized/degraded sufficiently to support the leakage of the contents of the cells. On the other hand, at high percentage of acetonitrile, evaporation of the extraction solution is too fast, and – as a result – the extraction time is too short, and the amounts of extracted metabolites are insufficient to produce intense MS signals. It should also be pointed out that – unlike the common extraction protocols used in metabolite analysis – the on-target extraction is almost completely passive, *i.e.* without prior sample degradation, grinding, shaking, or stirring. Metabolites need to be extracted despite the presence of the outer chorion layer protecting the egg. Although many standard protocols include the removal of the outer layer, the *in-situ* extraction process was conducted without prior dechoriation of the eggs. Based on the preliminary experiments, the outer protective layer of the eggs did not stop extraction of metabolites, and relatively high MS signals could be recorded (**Figure 2.2**).

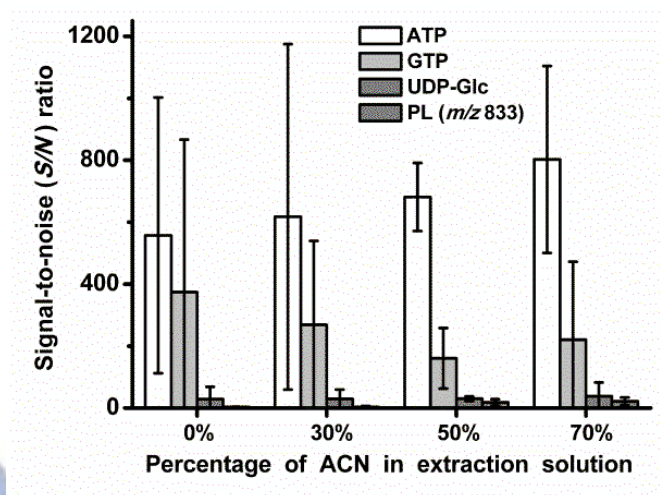


**Figure 2.3.** Influence of the concentration of acetonitrile (ACN) in the extraction solution on the *signal-to-noise* (*S/N*) ratios. This experiment included several metabolites (ATP, *m/z* 506; GTP, *m/z* 522; UDP-glucose, *m/z* 565; and a phospholipid, *m/z* 833) extracted from single eggs, and analyzed by MALDI-MS.

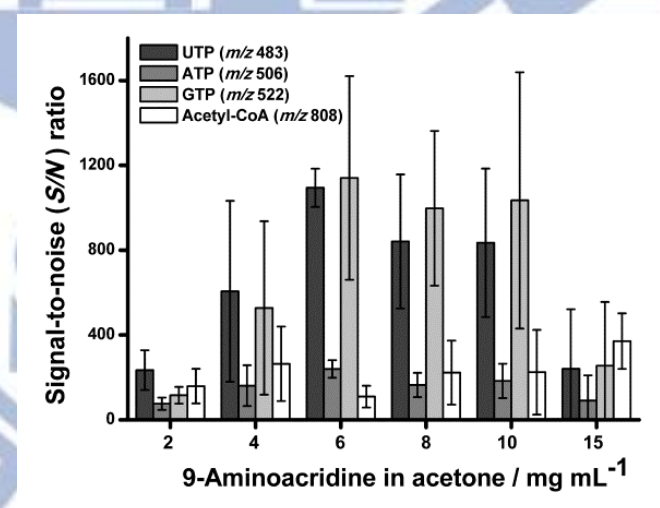


**Figure 2.4.** Influence of the concentration of the 9-aminoacridine matrix solution (in acetone) on the *signal-to-noise* (*S/N*) ratios of the peaks of various standard compounds. We found that at 6 mg mL<sup>-1</sup> 9-aminoacridine (in acetone), the *S/N* value is highest. Therefore, we chose this concentration of 9-aminoacridine for further experiments.

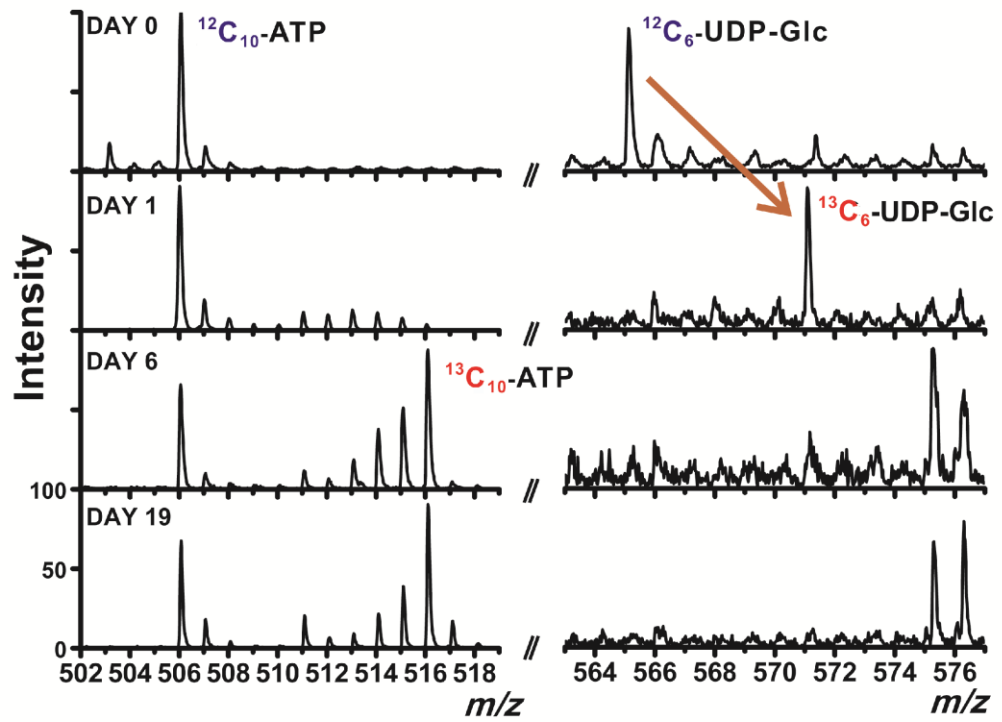


### 2.3.2 Isotopic labelling of fruit flies

When  $^{13}\text{C}_6$ -glucose is administered to fruit flies as the only carbon source, the  $^{13}\text{C}$  atoms are gradually incorporated into cellular metabolites. **Figure 2.5A** shows the outcome of labelling over 1, 6 and 19 days. We found that – using 1%  $^{13}\text{C}$ -glucose solution as the only carbon source – uridine diphosphate glucose (UDP-Glc) is promptly labelled with  $^{13}\text{C}$ , while the labelling of other metabolites – for example, adenosine triphosphate (ATP) – is much slower, and it does not reach completion during several days of incubation. The latter is concluded based on the presence of the non-labelled form of ATP after 19 days (the peak at the  $m/z$  506 in **Figure 2.5A**). Conversely,  $^{13}\text{C}$ -labeled glucose can readily replace the unlabelled glucose moiety in the molecule of UDP-Glc. Initially, the labelling of UDP-Glc is limited to the glucose ( $\text{C}_6$ ) moiety, while the UDP moiety remains unlabeled. Biosynthesis of UDP-Glc using UTP and glucose as substrates involves only two reactions, which are catalyzed by two enzymes: hexokinase (EC 2.7.1.1) and UTP-glucose-1-phosphate uridylyltransferase (EC 2.7.7.9; **Figure 2.5B**).<sup>44,45,46</sup> This gives the possibility of using partial isotopic labelling of UDP-Glc as an indicator of the early stages of primary metabolism while  $^{13}\text{C}_6$ -glucose is the only carbon source available. On the other hand, *de-novo* biosynthesis of adenosine triphosphate (ATP) involves multiple biotransformations, thus only several carbons can be replaced in most ATP molecules during several days of incubation.

In order to confirm the incorporation of carbon-13 to the UDP-glucose molecule, we implemented MALDI-MS/MS: As shown in **Figure 2.6**, the fragment of the non-labelled UDP-glucose (MS  $m/z$  565) was found to be non-labelled glucose phosphate (MS/MS  $m/z$  241).

A



B

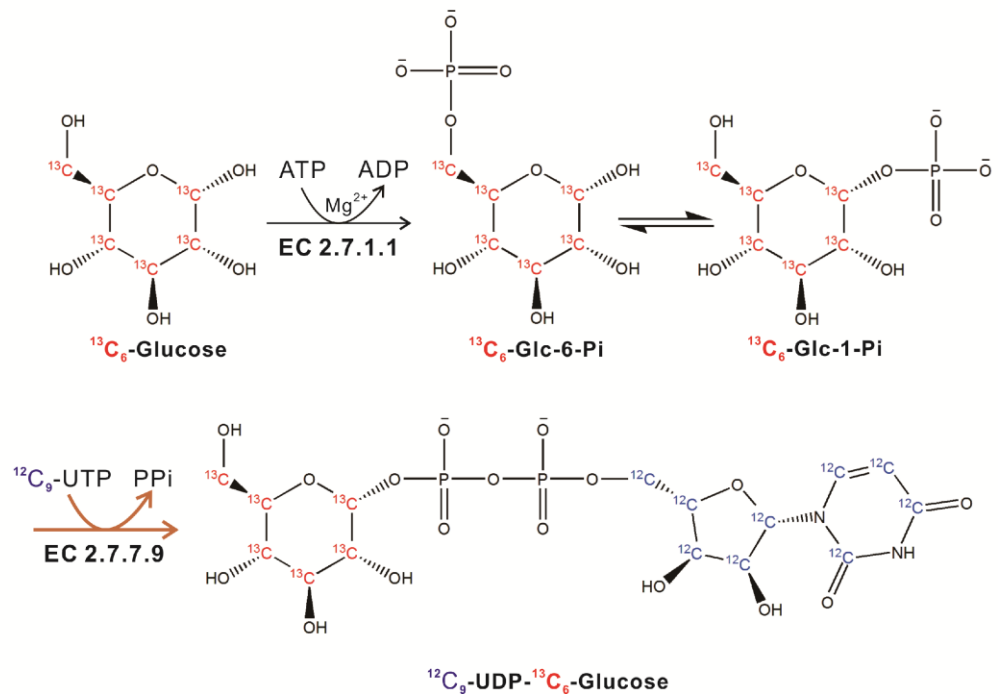


**Figure 2.5.** Isotopic labelling of ATP and UDP-Glc in single eggs. (A) MALDI mass spectra obtained from fruit flies following 1, 6, and 19 days of incubation with the  $^{13}\text{C}_6$ -glucose solution. (B) Reaction scheme of labelling glucose moiety in UDP-Glc with  $^{13}\text{C}_6$ -glucose.

The tandem MS analysis of the parent ion at the  $m/z$  571 (in a sample obtained from a labelled fly) revealed a shift of the fragment peak to the  $m/z$  247, which is due to the substitution of 6  $^{12}\text{C}$  atoms with  $^{13}\text{C}$  atoms in the glucose moiety of UDP-Glc. Since the mortality rate was high when the glucose solution was used as the only source of nutrients, we opted for short-term incubations ( $\leq 1$  day), and – in further experiments – we focused on the measurement of the labelling of glucose moiety in UDP-Glc molecules. It should be noted that UDP-Glc is represented by an MS peak ( $m/z$  565 or 571) that does not suffer from spectral/matrix interference.

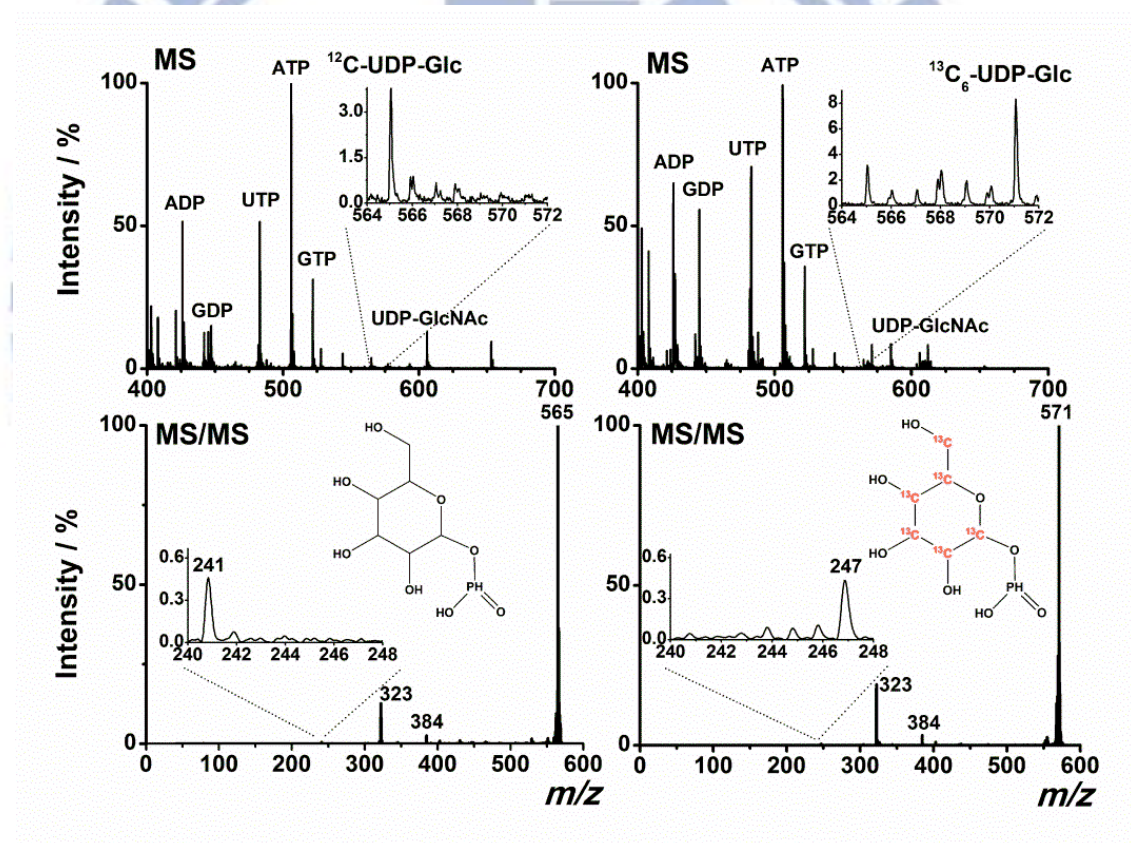


**Figure 2.6.** MALDI-MS and MS/MS analysis of metabolites in the eggs of fruit flies incubated with  $^{13}\text{C}$ -glucose.

Left: spectra for eggs obtained from flies incubated with  $^{12}\text{C}_6$ -glucose. Right: spectra for eggs obtained from flies incubated with  $^{13}\text{C}_6$ -glucose for 12 h. Evaluation of the MS/MS data was aided by the METLIN database (Scripps Center for Metabolomics, La Jolla, USA).

Using 9-aminoacridine matrix, it is also possible to detect other metabolites (*e.g.* adenosine diphosphate ( $m/z$  426), guanosine diphosphate ( $m/z$  442), adenosine triphosphate ( $m/z$  506), guanosine triphosphate ( $m/z$  522), uridine diphosphate glucose ( $m/z$  565), uridine diphosphate *N*-acetyl glucosamine ( $m/z$  606); **Figure 2.2**). Selecting UDP-Glc ( $m/z$  565) as a target analyte, we further want to show that MALDI-MS is readily applicable to detection of metabolic effects of environmental factors in fruit fly eggs. In future studies, one may also consider studying the labelling patterns of other metabolites by MALDI-MS. However, one can anticipate that the interpretation of results of such studies may not be as straightforward as in the case of UDP-Glc. Another point to consider is that when  $^{13}\text{C}$  atoms replace  $^{12}\text{C}$  atoms, the signal-to-noise ratios of the main peaks (corresponding to the unlabelled metabolites) are decreased due to isotopic dilution. Therefore, the experimental strategy described here is most applicable to analysis of metabolites represented by peaks with high signal-to-noise ratios.

### 2.3.3 Time course of UDP-Glc labelling

Subsequently, the time progress of the incorporation of 6  $^{13}\text{C}$  atoms to the glucose moiety of UDP-Glc in fruit fly eggs was studied. The incorporation of  $^{13}\text{C}$  to UDP-glucose takes approximately 20-30 h: during this time, a gradual increase of the ratio of the labelled UDP-Glc to the total (labelled + unlabelled) UDP-Glc can be observed (**Figure 2.7**). Based on the sigmoid function fitted to all the data points, the time ( $t_{1/2}$ ) after which the labelling of the studied population of eggs was 50% is estimated to be  $\sim 13$  h. A considerable variability of the labelling progress can be observed within the population of eggs analyzed at every time point (**Figure 2.7**). This variability will be discussed later on.



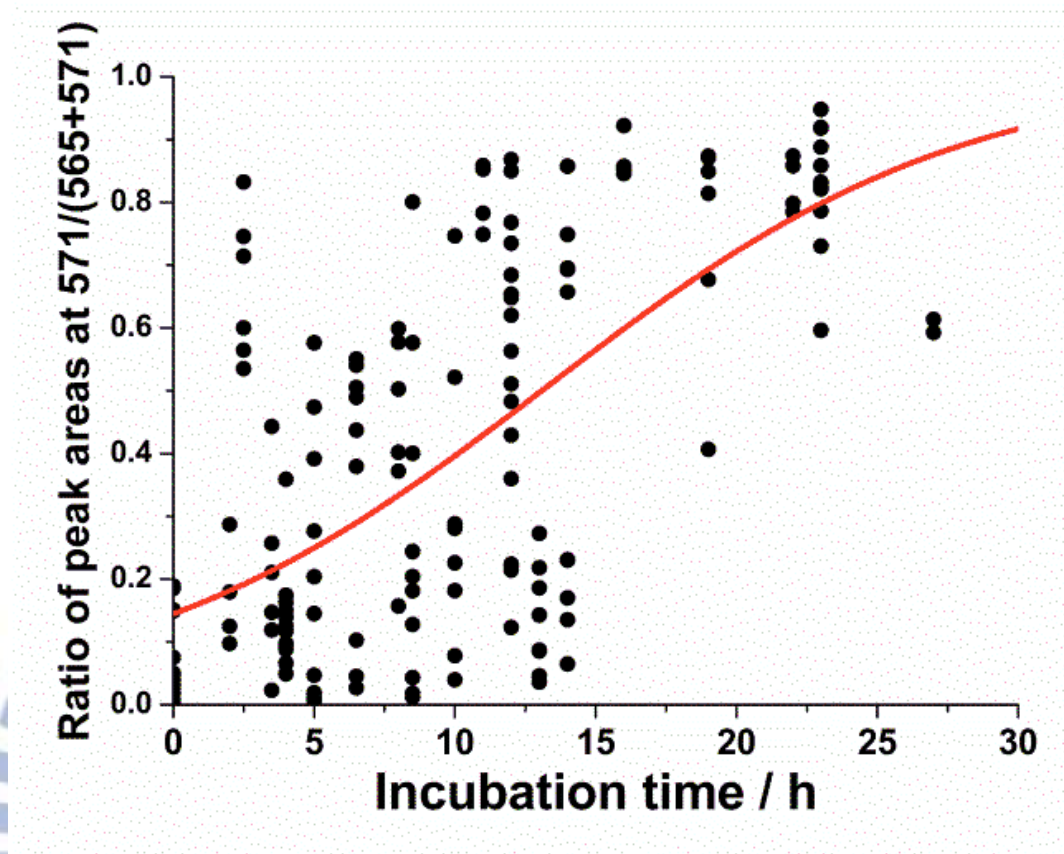


**Figure 2.7.** Progressive incorporation of the  $^{13}\text{C}$ -label to UDP-Glc in fruit fly eggs. The data points were fitted with a sigmoid function:  $y = 1.013 \cdot (1/(1+e^{(-0.135x+1.792)}))$ . During this experiment, the flies were incubated with  $^{13}\text{C}_6$ -glucose and illuminated with white light ( $\sim 4000$  lux). Note that the sampling intervals (as projected onto the  $x$ -axis) are coincidentally not constant.

It should also be pointed out that the application of matrix solution to the biological sample, and subsequent analysis in the vacuum compartment of MALDI mass spectrometer may cause some bias to the analytical result. However, this bias is greatly reduced by using isotopic labels: it is unlikely that the enzyme-catalyzed labelling process will proceed with high rate following the quenching of metabolism with acetonitrile used in the course of sample preparation.

### 2.3.4 Influence of the incubation conditions on the isotopic labelling of eggs

In the following experiment, we investigated the influence of temperature on the labelling of UDP-Glc. Two batches of female fruit flies were incubated under low (21 °C) and high (28 °C) temperature for 24 h; in both cases, light was on. Following the analysis by MALDI-MS, we found that the labelling level was significantly higher in the flies incubated at 28 °C, as compared with the flies incubated at 21 °C (**Figure 2.8**).

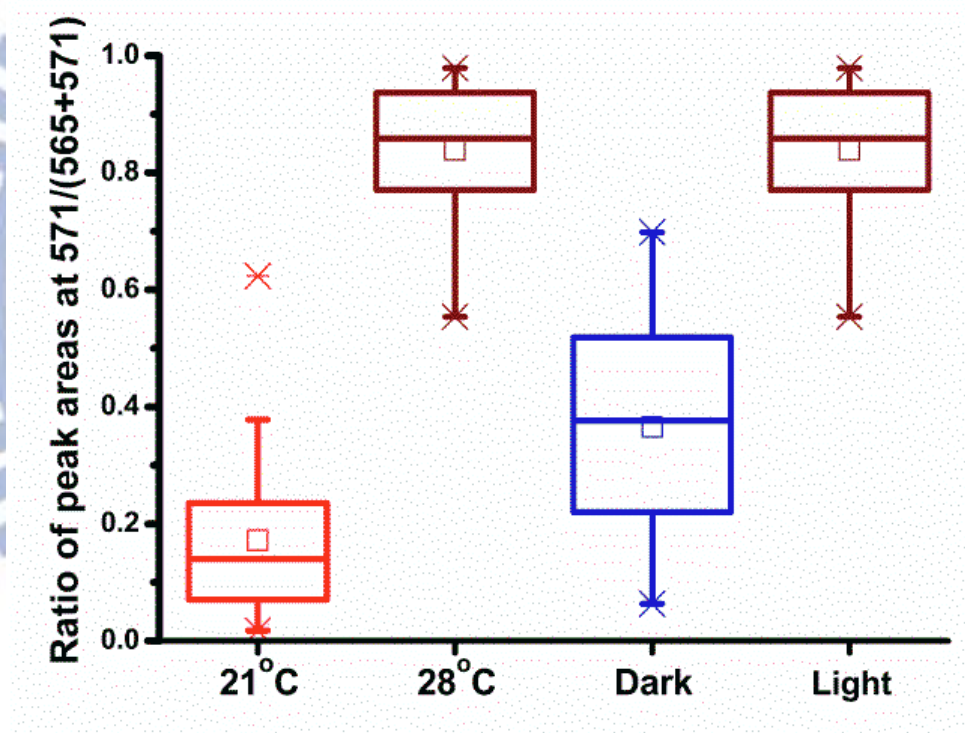


**Figure 2.8.** Influence of temperature (21 vs. 28 °C) and illumination (dark vs. light) on the labelling of glucose moiety in UDP-Glc molecules extracted from individual eggs. Female flies were incubated with  $^{13}\text{C}_6$ -glucose solution during 24 h. The default conditions were: white light on, ~ 4000 lux (in the study involving the change of temperature); temperature, 28 °C (in the study involving the change of illumination).

In another experiment, we also found that illuminating the batch of female flies during the incubation with  $^{13}\text{C}_6$ -glucose had strong effect on the labelling of UDP-Glc in eggs: the flies incubated in the dark metabolized much less  $^{13}\text{C}_6$ -glucose than the flies incubated under light (**Figure 2.8**). These observations highlight the feature of the proposed isotope label-aided mass spectrometric method: environmental factors (temperature, light) are reflected in the measured labelling yields of the target metabolite (UDP-Glc).

### **2.3.5 Influence of circadian adaptation on the labelling of eggs**

The mechanism of circadian clock has broadly been investigated: a number of previous studies pointed out activation of specific genes which are responsible for the maintenance of circadian rhythm in fruit fly.<sup>47,48</sup> In the present study, we investigated how the adaptation of fruit fly to light/dark cycle can affect the labelling of UDP-Glc in eggs, irrespective of the treatment (light on/off). It was also interesting to verify the effect of the alteration of the culture conditions – from normal (light on during circadian day) to abnormal (light off during circadian day). At the beginning, we entrained the flies with a 24-h light/dark cycle: the photoperiod of 12-h day (9:00 AM – 9:00 PM) / 12-h night (9:00 PM – 9:00 AM). Subsequent incubation with  $^{13}\text{C}_6$ -glucose began at the time when the light would be turned on or off: one batch of the flies was incubated under light for 12 h, and the other batch was incubated for 12 h in the dark, irrespective of the light/dark cycle applied during the entrainment period (before the actual experiment). The analysis of single eggs according to the protocol in **Figure 2.1** followed, and the results are summarized in **Figures 2.9-2.14**, and **Tables 2.1-2.3**.



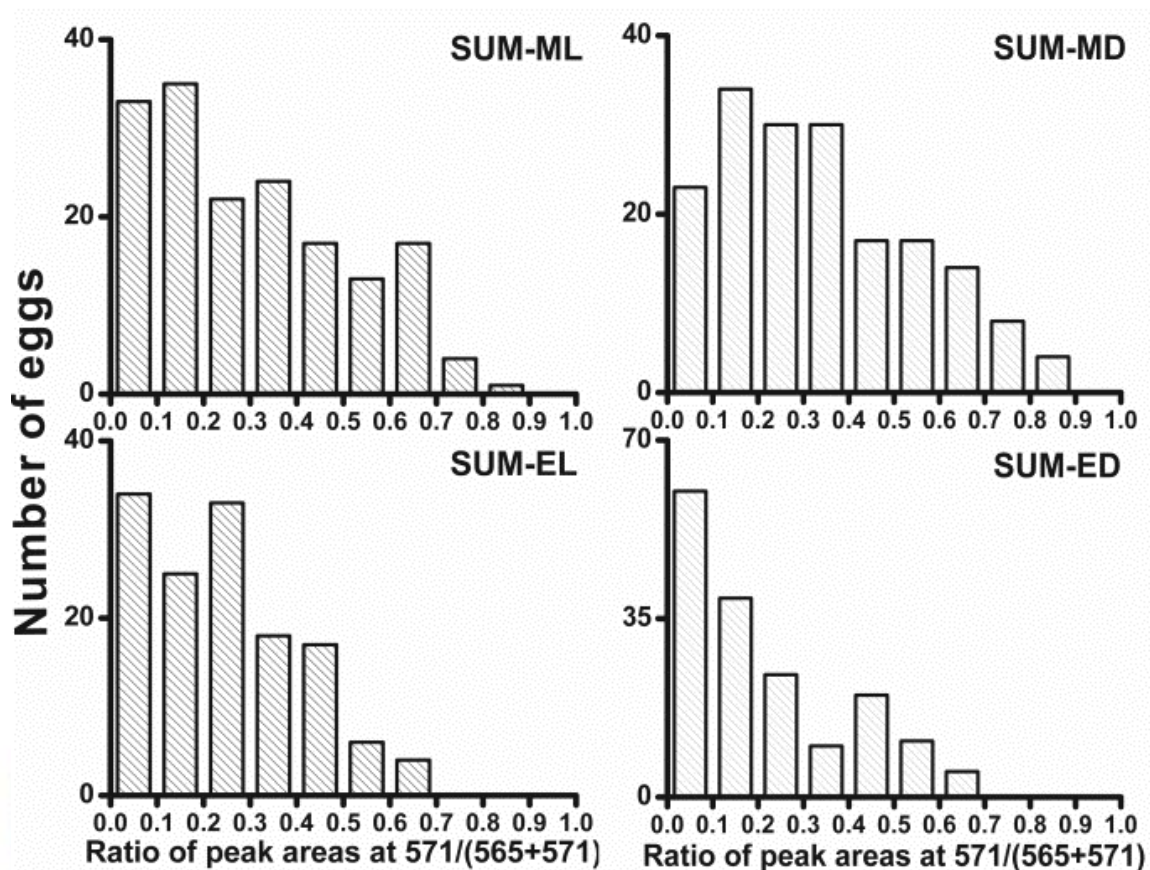


**Figure 2.9.** Histograms showing the distributions of labelling levels within the eggs obtained from the fruit flies incubated with  $^{13}\text{C}_6$ -glucose (during 12 h) at different illumination conditions and at different times during the day/night cycle. ML – flies incubated during day (starting from the morning) at light; MD – flies incubated during day (starting from the morning) at dark; EL – flies incubated during night (starting from the evening) at light; ED – flies incubated during night (starting from the evening) at dark.

We found that – compared with the flies incubated under normal conditions (light on during day; ML) – the flies incubated under abnormal conditions (light off during day; MD) exhibited similar metabolic activity, *i.e.* in accordance with their biological clock which had been adjusted during the entrainment period. Based on the results of the one-sample Kolmogorov-Smirnov test, we found that none of the data sets in **Figure 2.9** follows normal distribution. Due to the fact that the labelling is not complete within the 12-h period,



corresponding to either circadian day or night (*N.B.* the labelling “half life” at full light:  $t_{1/2} \approx 13$  h), the distributions are asymmetrical and have right-side tails (*Skewness* > 0; **Table 2.1**).

**Table 2.1.** Statistical data on the samples analysed in this study. ML – flies incubated during day (starting from the morning) at light; MD – flies incubated during day (starting from the morning) at dark; EL – flies incubated during night (starting from the evening) at light; ED – flies incubated during night (starting from the evening) at dark.

	ML	MD	EL	ED
Number of repeats	5	5	5	5
Total number of flies	31	30	27	28
Total number of eggs ( <i>n</i> )	166	177	137	169
Mean	0.306	0.338	0.245	0.214
Median	0.267	0.399	0.278	0.444
Standard deviation	0.207	0.211	0.164	0.177
Skewness	0.517	0.536	0.657	0.811
Kurtosis	2.20	2.26	2.78	2.47

Further statistical analysis using the two-sample Kolmogorov-Smirnov test (TSKST) revealed that depriving the fly stock of light during the circadian day (ML vs. MD) did not produce a significant change in the distribution of the labelling level of UDP-Glc within a large sample of fly eggs; in other words, the null hypothesis that the ML and MD data sets (**Figure 2.9**) are from the same continuous distribution was not rejected at the 5% significance level (TSKST  $p = 0.3226$ ; **Table 2.2**).

**Table 2.2.** Results ( $p$ -values) of the two-sample Kolmogorov-Smirnov test performed on the data obtained in this study. ML – flies incubated during day (starting from the morning) at light; MD – flies incubated during day (starting from the morning) at dark; EL – flies incubated during night (starting from the evening) at light; ED – flies incubated during night (starting from the evening) at dark. Null hypothesis: the two data sets are from the same continuous distribution. Red colour indicates the  $p$ -values where the null hypothesis is rejected (at the 5% significance level).

	ML	MD	EL	ED
ML	1.0000	0.3226	0.0157	0.0002
MD	0.3226	1.0000	0.0042	~0.0000
EL	0.0157	0.0042	1.0000	0.0172
ED	0.0002	~0.0000	0.0172	1.0000

Another non-parametric test (Wilcoxon rank sum test, WRST) did not reject the null hypothesis that the ML and MD data sets are drawn from identical continuous distributions with equal medians (WRST  $p = 0.1334$ ). In addition, the percentage of eggs with a high labelling level ( $\geq 0.5$ ) in the samples collected after day-time incubation was comparable in the light- and dark-incubated flies: 21 and 24%, respectively (**Table 2.3**).

**Table 2.3.** Numbers of eggs with the labelling level higher or equal to 0.5 in each of the four groups. ML – flies incubated during day (starting from the morning) at light; MD – flies incubated during day (starting from the morning) at dark; EL – flies incubated during night (starting from the evening) at light; ED – flies incubated during night (starting from the evening) at dark.

	ML	MD	EL	ED
Number of eggs with labelling level $\geq 0.5$	35	43	10	16
Share in the total (%; cf. <b>Table S1</b> )	21	24	7	9

Statistical analysis further revealed that the distributions of the data points from the day/light (ML) incubation and the night/light (EL) incubation are different (TSKST  $p = 0.0157$ ; **Table 2.2**). The data set obtained for the day/dark (MD) incubation also reflects a different distribution than the data set obtained for the night/dark (ED) incubation (TSKST  $p \approx 0.0000$ ; **Table 2.2**). The percentage of the eggs with a high labelling level ( $\geq 0.5$ ) was lower for the flies incubated with  $^{13}\text{C}_6$ -glucose during night (7 and 9%) than during day (21 and 24%), irrespective of the presence of light (**Table 2.3**). Providing light to the flies during circadian night (EL vs. ED) slightly affected the labelling distribution in the studied sample of eggs (TSKST  $p = 0.0172$ ; **Table 2.2**). This may suggest that the illumination of the fly stock against the entrained circadian rhythm (*i.e.* “light on” during night) has a greater influence on metabolic activity than light deprivation (*i.e.* “light off” during day). Overall, based on the above results, we conclude that the metabolism of fruit flies reared under altered illumination follows the internal circadian rhythm, which was learned during the entrainment period preceding the incubation with  $^{13}\text{C}_6$ -glucose. The internal circadian rhythm dominantly controls the metabolic activity of eggs – as quantified based on the level of  $^{13}\text{C}$  incorporated to UDP-Glc – despite an acute perturbation to the dark/light cycle.

The differences in the isotopic labelling of eggs raise discussion about the possible source of the dependencies of the labelling rates on the temporal phases within circadian rhythms. In fact, fruit fly exhibits a circadian rest-activity cycle with prolonged intervals of rest, which share many features with mammalian sleep.<sup>32,49</sup> Previously, the physical activity of fruit flies was studied with a specially designed locomotor assay, which quantifies physical movements of flies.<sup>50</sup> The experimental approach implemented in the present work allowed us to obtain information about biosynthesis of one particular metabolite (UDP-Glc). Due to the high labelling rates, observation of the labelling progress during short incubation periods

(12 h) was possible (**Figure 2.7**). The differences in the results obtained following the incubation of flies with  $^{13}\text{C}$ -Glc at different times, and at different illumination (*e.g.* day/light – ML *vs.* night/dark – ED), may be due to the following reasons: (i) Locomotion of fruit flies is greater during circadian day than during circadian night,<sup>32</sup> therefore the probability that the individual flies encounter the reservoir with the solution of  $^{13}\text{C}$ -labelled glucose, and ingest the isotopically labelled carbohydrate, is greater during day than at night. (ii) Physiological and metabolic activity of individual flies is higher during circadian day than during circadian night, despite the altered light/dark cycle.

To the best of our knowledge, the present study is the first one that reveals short-term metabolic effects in metazoan eggs due to circadian adaptation. In future, it would be appealing to develop other microscale assays that would provide complementary data on molecular composition of individual eggs, and gain further insight to the influence of circadian adaptation on egg metabolism. To this end, one promising experimental approach – complementary to the current one – could be the implementation of microscale nuclear magnetic resonance.<sup>51</sup>

### 2.3.6 Labelling variability

In a previous work, stable isotopes were used to study embryonic proteome in fruit fly: pooled samples – composed of multiple embryos – were analyzed.<sup>40</sup> The current study provides information about metabolic activity of individual eggs obtained directly from fly bodies by dissection. While the histograms in **Figure 2.9** present the data for large numbers of flies (> 25) and eggs (> 130), it is also interesting to look into the egg-to-egg and/or fly-to-fly variability, which have already become apparent in the labelling time-course study (**Figure 2.7**). The fly-to-fly variability is illustrated within histograms plotted separately for each fly



included in the study (**Figures 2.10** and **2.11-2.14**). For example, in **Figure 2.10** one can easily spot differences between individuals (different histograms), and eggs (multiple bars in the histograms).

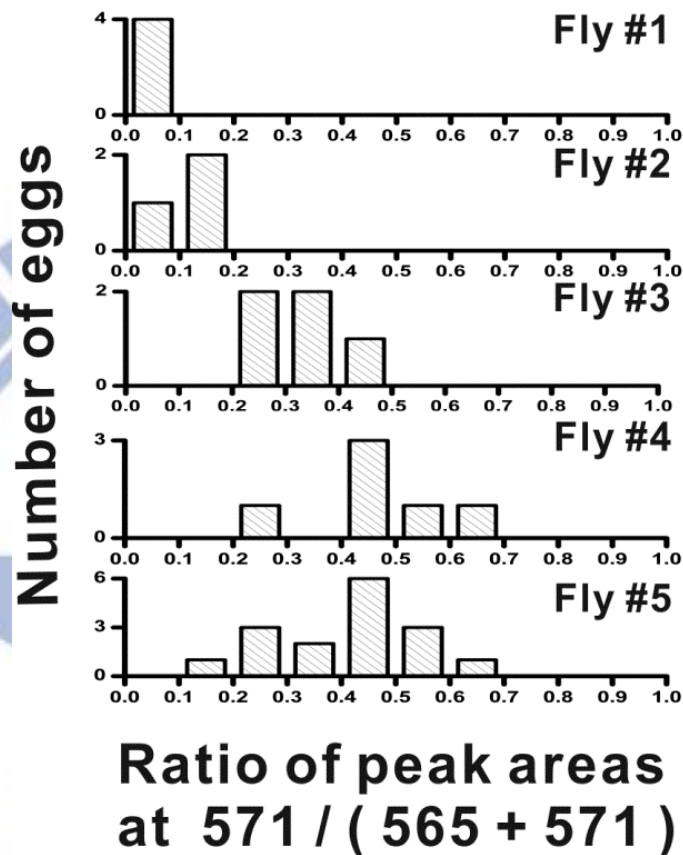


**Figure 2.10.** Histograms showing differences in the labelling of eggs among flies from the same treatment. Flies incubated during night (starting from the evening) at dark (ED): arbitrarily selected examples of five single-fly histograms, ordered according to the increasing level of labelling (Fly #1 to #5: top to bottom). All single-fly histograms from this experimental variant are displayed in **Figure 2.14**.

Although the distribution of labelling in the whole population of fly eggs within one treatment appears flat (for example, **Figure 2.12**, red bars, for the MD group; *Kurtosis* = 2.26, **Table 2.1**), the average labelling levels which can be calculated for eggs obtained from every fly are different. These differences are probably the result of phenotypic variability within the population of fruit flies included in this experiment. Close examination of the single-fly

histograms in **Figures 2.10** and **2.14** – representing the flies incubated during night at dark (ED) – leads to an observation that although most flies did not incorporate much carbon-13 into their eggs (*e.g.* Flies #1 and #2 in **Figure 2.10**), there are several outliers – flies with notably higher labeling yield (*e.g.* Flies #4 and #5 in **Figure 2.10**). While comparable data sets – showing the influence of circadian rhythms on primary metabolism of individual eggs or embryos, and tissue cells – cannot be found in scientific literature, it is worthwhile mentioning that in a study conducted using mouse model, strong heterogeneity of circadian entrainment kinetics was found not only between different organs, but also within the molecular clockwork of each tissue.<sup>52</sup>

It should also be pointed out that eggs from single fly are exposed to the same concentration of  $^{13}\text{C}_6$ -glucose; consequently, egg-to-egg variability of the labelling ratios (peak areas at the  $m/z$  571/(565+571)) is an intrinsic property of eggs – independent of fly activity and glucose consumption. In each of the single-fly histograms (**Figures 2.11-2.14**, black bars), one can also see the distributions of the labelling ratios within each of the flies studied. The average spreads of the labelling distribution within the population of eggs in every fly included in each treatment were:  $0.32 \pm 0.15$  (s.d.),  $0.29 \pm 0.11$  (s.d.),  $0.25 \pm 0.10$  (s.d.), and  $0.26 \pm 0.15$  (s.d.) in ML, MD, EL, and ED, respectively. Thus, the spreads of the labelling ratios in every fly are typically much smaller than the spread of the labelling ratio calculated for the whole population of eggs included in the analysis: 0.9, 0.9, 0.7, and 0.7 in ML, MD, EL, and ED, respectively (**Figures 2.11-2.14**, red bars); with a tendency towards a higher egg-to-egg variability in the flies incubated with  $^{13}\text{C}_6$ -glucose during circadian day.

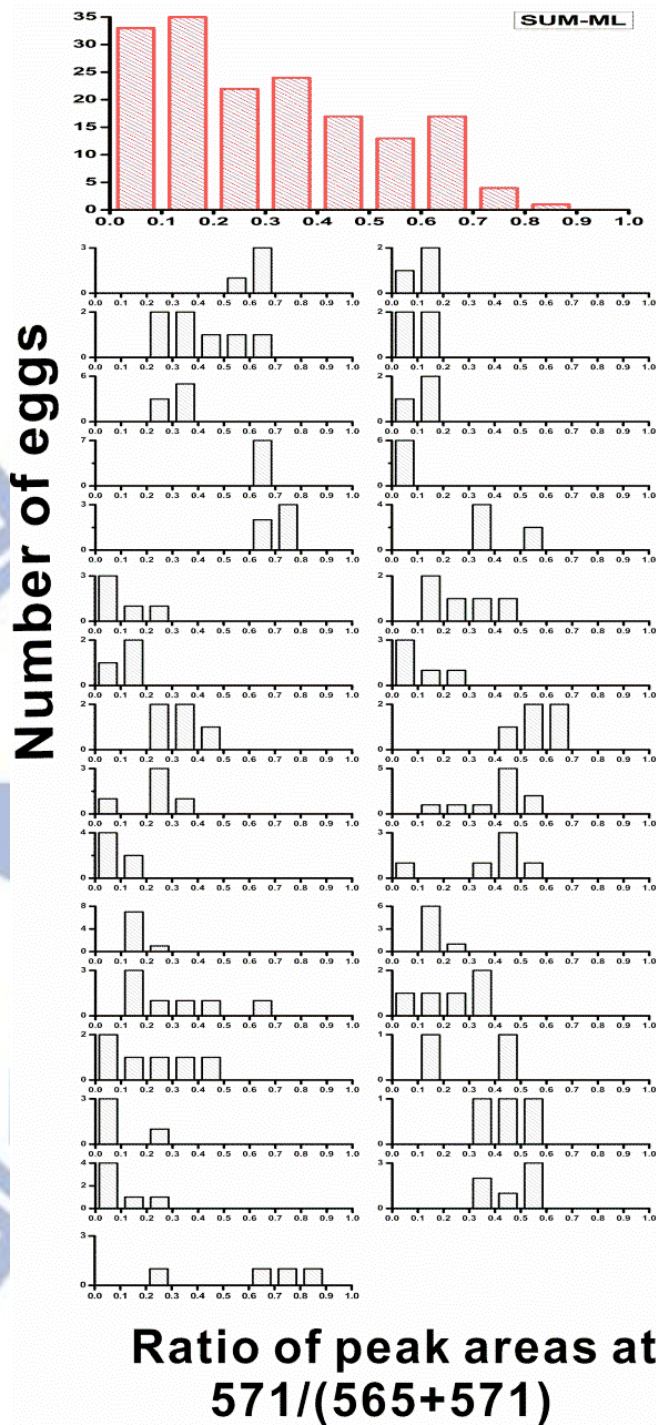


**Figure 2.11.** Histograms showing differences in the labelling of eggs among flies from the same treatment (ML – flies incubated during day (starting from the morning) at light; black bars). Each of the small histograms (black bars) corresponds to a single fruit fly. The cumulative histogram for all the eggs obtained from the ML treatment (red bars).



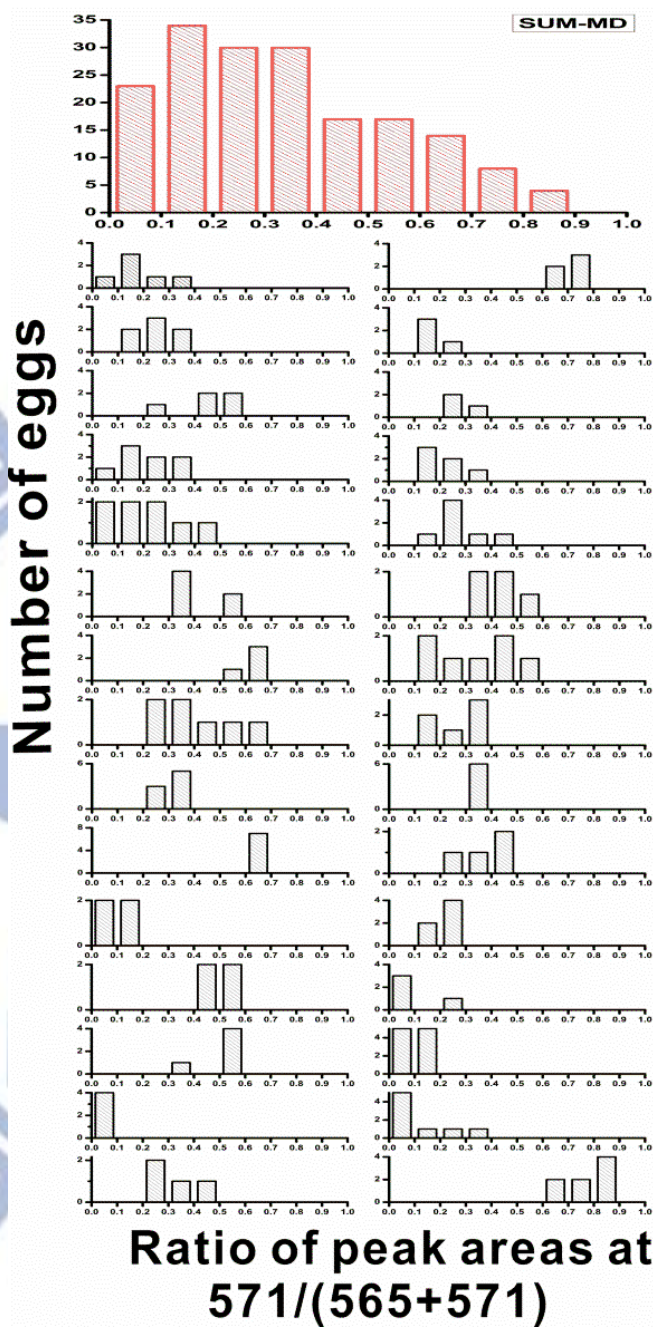


**Figure 2.12.** Histograms showing differences in the labelling of eggs among flies from the same treatment (MD – flies incubated during day (starting from the morning) at dark; black bars). Each of the small histograms (black bars) corresponds to a single fruit fly. The cumulative histogram for all the eggs obtained from the MD treatment (red bars).



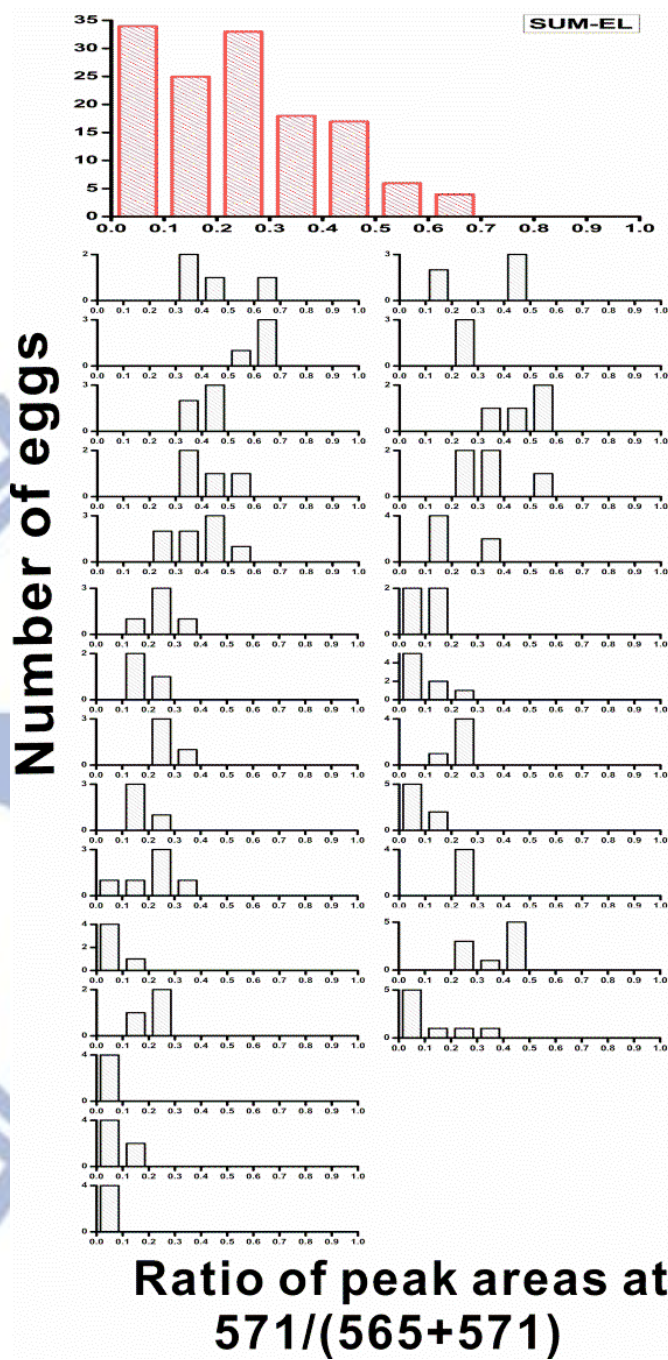


**Figure 2.13.** Histograms showing differences in the labelling of eggs among flies from the same treatment (EL – flies incubated during night (starting from the evening) at light; black bars). Each of the small histograms (black bars) corresponds to a single fruit fly. The cumulative histogram for all the eggs obtained from the EL treatment (red bars).

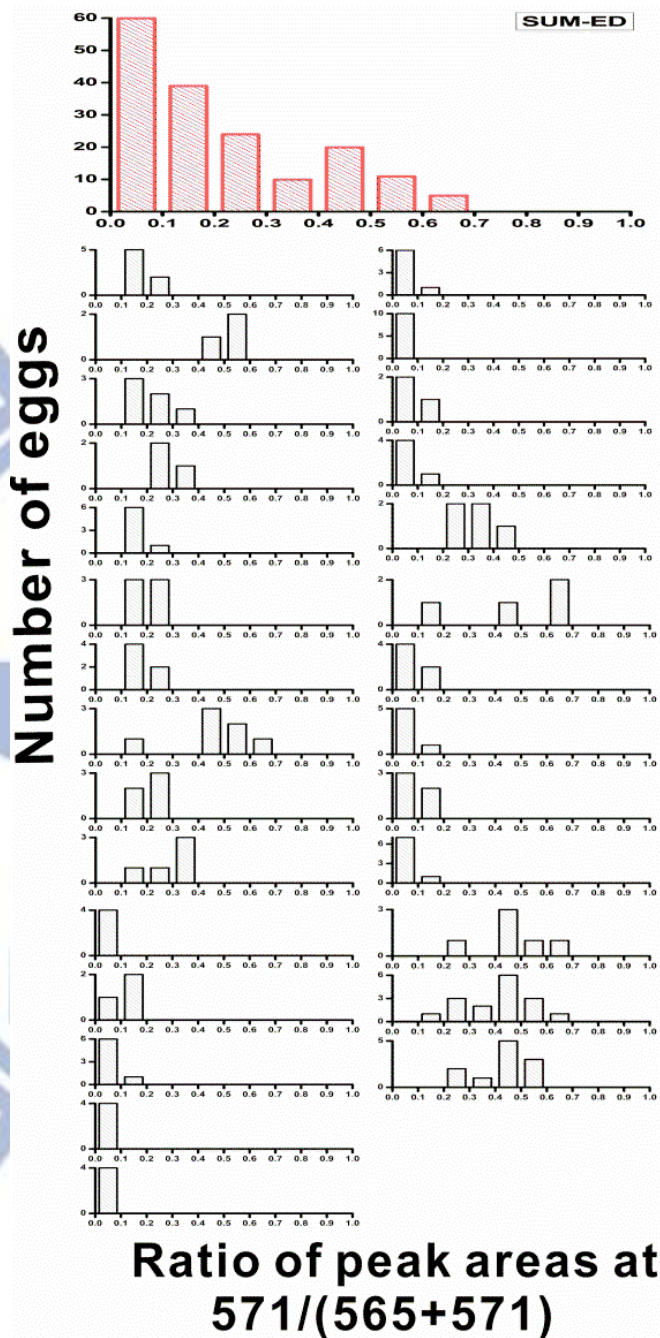


**Figure 2.14.** Histograms showing differences in the labelling of eggs among flies from the same treatment (ED – flies incubated during night (starting from the evening) at dark; black bars). Each of the small histograms (black bars) corresponds to a single fruit fly. The cumulative histogram for all the eggs obtained from the ED treatment (red bars). Selected histogram from this figure are also displayed in **Figure 2.10**.

## 2.4 Concluding remarks

The study has shown the feasibility of isotopic labelling of fruit flies with the purpose of pursuing metabolic effects of the circadian clock and environmental cues by mass spectrometry. It has demonstrated a link between the circadian clock and the egg metabolism in fruit fly. The results reveal a substantial metabolic inertia of the circadian clock: once adapted to the day/night cycle, the incorporation of  $^{13}\text{C}$  to UDP-Glc was not significantly altered by acute perturbation of the illumination cycle. The proposed MALDI-MS and stable isotope-aided protocol was found to produce useful information which reflects the treatment applied to the fly stocks. The main advantage of this experimental approach is that quasi-quantitative data sets can be obtained for single eggs without elaborate sample preparation. Instead of performing absolute quantification of individual metabolites – the ratio of the MS signal corresponding to the labelled metabolite and the sum of the MS signals corresponding to the labelled and the unlabelled metabolite can be used as the proxy for metabolic activity. We believe this method will help to explore other biochemical phenomena related to metabolism in fruit fly as well as other metazoan species (for example, *Caenorhabditis elegans*), which are considered as model organisms in biology.



# CHAPTER 3:

## Facile sampling of sweat combined with direct analysis of metabolites by nanoDESI-MS

---

### 3.1 Background

Clinical analysis deals with detecting metabolites excreted by human body. The chemical profiles of bodily excretions can inform doctors about the health status of their patients. Urine is one of the most frequently analyzed clinical samples. However, sampling urine is not always convenient or possible. Besides urination, sweating is another way of excreting substances from body. So far, there has been less progress in the use of sweat samples in diagnosis – probably due to the technical difficulties associated with sampling and analysis. However, sampling and analyzing sweat can be advantageous for clinical diagnostics.<sup>53,54,55</sup> In principle, sweat samples may be collected almost any time. In previous studies, chromatographic methods were used to analyze metabolites in sweat samples.<sup>53,54,55,56</sup> The advantage of using chromatography is the easiness of separation of numerous metabolites. Gas chromatography is particularly useful in the analysis of volatile metabolites, and it can readily be coupled with solid-phase microextraction (SPME) for preconcentration of less abundant analytes. The results of study using GC showed the possibility of detecting numerous metabolites.<sup>57,58</sup> However, GC analysis is time-consuming. In this study, we attempt to use mass spectrometry in direct detection of sweat metabolites collected directly from skin using passive sampling tools.



In order to perform fast MS-aided analysis of sweat samples, we considered using one of the available atmospheric-pressure ion sources. For example, in 2004, Prof. Graham Cooks and co-workers introduced desorption electrospray ionization (DESI) mass spectrometry, in which the analytes are lifted from solid surfaces using a stream of charged microdroplets.<sup>59</sup> This technique enables soft ionization of biomolecules. Commercial mass spectrometers can be used in conjunction with DESI source without any modification, which made this technique particularly promising for this project. However, despite elaborate optimization, the preliminary experiments conducted as a part of this study showed that the DESI technique is difficult to reproduce, and the sensitivity is not sufficient to fulfill the requirements if the project focused on the analysis of sweat samples deposited on solid surfaces.

Another promising ionization technique, which was also introduced quite recently, is the nanospray desorption electrospray ionization (nano-DESI).<sup>60</sup> The nanoDESI setup consists of two microscale capillaries: one is used to deliver the nanoDESI solvent mixture to the sample, whilst the other one is used to transfer the solubilized samples towards the MS in the form of electrospray plume. These two capillaries are joined by a bridge of the nanoDESI solvent, which ensures continuity of sample extraction and ionization. Compared to DESI, in nanoDESI the extraction of the analyte and the ionization are separated in space.<sup>61</sup> The nanoDESI source has a very simple design, and can easily be constructed almost in any laboratory. According to the recent reports, nanoDESI has been used in the studies in environmental chemistry like composition of organic aerosols in the air,<sup>62</sup> mass spectrometric imaging of plant tissues,<sup>63</sup> and the analysis of dried blood spots.<sup>64</sup> The authors of these reports have emphasized that nanoDESI is a reliable ion source, and comparable with DESI.<sup>62, 63, 64</sup>

For a better understanding of the nanoDESI concept, it is also helpful to compare it with two other ion sources: nano-electrospray ionization (nanoESI) and contactless atmospheric pressure ionization (CAPI). NanoESI is a widely used ion source for conducting mass spectrometric measurements on samples delivered at atmospheric pressure. Since it was introduced by Dr Matthias Wilm in 1996, it has immediately become a common-use ion source with many applications.<sup>65</sup> The nanoESI source uses very low flow rates (down to ~ 10 nL min<sup>-1</sup>). Very small droplets are generated at the tip of nanoESI emitter while no nebulizer gas is applied. Tiny amounts of samples as 0.2-2 μL can be analyzed using this ion source.<sup>66</sup> In essence, the nanoDESI emitter resembles the nanoESI emitter. The difference is that nanoDESI accommodates analysis of solid samples which are extracted on-line, just before the ionization step. In 2011, Prof. Yu-Chie Chen and co-workers developed a new type of ion source, which they termed “contactless atmospheric pressure ionization” (CAPI).<sup>67</sup> Similar to nanoESI, CAPI also incorporates a tapered capillary emitter; however, the latter approach does not require establishing direct electric contact with the power supply. Real samples, such as fruit, can be analyzed with little or no pre treatment. The short capillary emitter is capable to spray the charged droplets without applying any external force; in fact, in the first study,<sup>67</sup> the main driving force was capillary action. Therefore, the CAPI system also resembles the second section (close to the MS inlet) of the nanoDESI setup. Similarly to CAPI, the nanoDESI setup does not feature electrical connection of the spray emitter with a power supply. Unique to nanoDESI is the possibility of extracting solid samples adsorbed on surfaces *in situ* prior to ionization. Therefore, this technique seems ideal for detection of metabolites adsorbed on surface of passive sweat samplers.

In this study, we first aimed to construct a nanoDESI source, and couple it with MS. Subsequently, the setup had to be tested with standard compounds. Second, we wanted to

verify if it is possible to detect metabolites adsorbed on the sampling tools by using this technique. Here we have taken advantage of commercial plasters as a ready material for the collection of sweat samples. We believed that the plasters are good enough for collecting and concentrating metabolites secreted with sweat, and could also be compatible with the nanoDESI-MS platform. Besides the commercial plasters, we also tested other materials, such as Teflon tape and filter paper.

## **3.2 Experimental section**

### **3.2.1 Materials**

Acetic acid, 9-aminoacridine and creatinine were purchased from Sigma-Aldrich (St Louis, USA). Acetonitrile (LC grade) and methanol (LC-MS grade) were purchased from Merck (Darmstadt, Germany). Urea was purchased from JT Baker (Phillipsburg, USA). Palmitic acid was purchased from Alfa Aesar (Massachusetts, USA).






### **3.2.2 Collecting real samples**

A 25-y/o healthy male – a non-smoker, not addicted to drugs or alcohol – volunteered to donate sweat samples for the study. The samples were collected several times – either directly to a test tube, or by using sampling materials listed in **Table 3.1**. The first samples used in this work were obtained following ~ 1 h of uninterrupted exercise in the gym. The plaster A was attached to skin near elbow. After the exercise, sweat was also collected to a test tube. The liquid samples were purified by centrifugation at 8000 rpm for 20 min. Subsequently, the

supernatant was diluted three times with pure methanol (LC-MS grade). Eventually, the solution was filtered using a 0.22- $\mu\text{m}$  porous syringe filter, and stored in the refrigerator.

The other samples were collected in the morning: The volunteer consumed several cookies, drank a cup ( $\sim 100$  mL) of black coffee, and attached the plaster onto their arm (near their elbow). After  $\sim 1$  h, the plaster was taken away, and used as sample in the experiments. Alternatively, the plasters were stored in the freezer at  $-4$   $^{\circ}\text{C}$ .

**Table 3.1.** Features of the sampling materials used in this study.

Code	Manufacturer	Type	Appearance	Picture
A	3M	Nexcare bandage	Non-transparent	
B	3M	Nexcare waterproof bandage	Transparent	
C	ASO Pharmaceutical	Fabric bandage	Non-transparent	
D	Toyo Roshi Kaiaha	Filter paper, qualitative No. 2	White paper	
E	TBL	Thread-seal Teflon tape	White and thin	



### 3.2.3 Construction of the nanoDESI source

The nanoDESI system was built according to the original design reported by Laskin and co-workers.<sup>6</sup> **Figure 3.1** shows the setup used in this work: syringe pump was used to deliver nanoDESI solvent into the junction of two capillaries. A short fused silica capillary (length 2 cm, ID 150  $\mu\text{m}$ , OD 360  $\mu\text{m}$ ) was positioned such that a liquid junction could be formed between its inlet and the outlet of the capillary used to deliver nanoDESI solvent. Electrical connection with the ground was established at the metal needle of the syringe mounted in the syringe pump, and no other electrical connection was in use. The angle between the solvent capillary and the nanoDESI emitter was set to  $\sim 45^\circ$ . The nanoDESI emitter was initially tapered by pulling the fused silica capillary in flame, as described previously.<sup>67,68</sup> The distance between the outlet of the nanoDESI emitter and the MS inlet was set to  $\sim 1$  mm. All the devices were placed on a one-axis translation stage for easy adjustment. The nanoDESI samples (*e.g.* plasters) were attached onto glass slides and fixed to an XYZ-stage to enable precise adjustment of the sampling position during the nanoDESI-MS measurement. The solvent mixture used in this nano-DESI experiment was composed of methanol and acetonitrile with the volume ratio 1:1, spiked with acetic acid (final concentration,  $\sim 0.1\%$ ). The flow rate of the nanoDESI solvent was set to  $2\text{-}5 \mu\text{L min}^{-1}$  (depending on experiment).

### 3.2.4 Mass spectrometry instrumentation

During the mass spectrometric analysis, we used the amaZon speed ion trap mass spectrometer from Bruker Daltonics (Bremen, Germany). The analyses were conducted with the voltage applied at the MS transfer capillary inlet set at  $-4.5$  kV or  $+4.5$  kV when working

in the positive and negative-ion mode, respectively. The dry gas flow rate was set to 10 L min<sup>-1</sup>. The  $m/z$  range was normally set to 20 – 400.

### 3.2.5 Data processing

The MS data were acquired using the DataAnalysis software (version 4.0; Bruker Daltonics), then treated and displayed using the Origin Pro software (version 8; Origin Lab Corporation, Northampton, USA).

## 3.3 Results and discussion

### 3.3.1 Setup of the nanoDESI-MS system

In our attempt to build a nanoDESI source, we followed the article by Roach *et al.*<sup>60</sup> (see Experimental Section; **Figure 3.1**). Several points of the ion source design and construction should be highlighted: The nanoDESI emitter capillary was tapered in the flame of a burner. Sharpening the outlet of the nanoDESI capillary helped to generate small microdroplets which are amenable to desolvation. In order to ascertain a high stability of the liquid junction between the two capillaries of the nanoDESI setup, and ensure continuity of the flow line, the flow rate had to be chosen carefully in a series of preliminary experiments (data not shown). The flow rate was also adjusted taking into account the wettability of the sample support with nanoDESI solvent. For instance, when analyzing samples adsorbed on the glue-coated section of plaster, we used a relatively low flow rate, 3  $\mu\text{L min}^{-1}$ . When using hydrophilic materials, such as filter paper, we had to use higher flow rates (*e.g.* 20  $\mu\text{L min}^{-1}$ ), so as to ensure a high stability of the liquid junction. Furthermore, in order to keep the signal stable, we also had to make sure that there were no gas bubbles present in the flow line.

Owing to the design of the ion trap mass spectrometer, the high voltage  $-4.5$  kV or  $+4.5$  kV was applied at the inlet of the instrument. Therefore, in the nanoDESI setup, we connected electrical ground with the needle of the syringe used to pump nanoDESI solvent. We found that the electrical grounding of the method needle contributed to a higher stability of signal (data not shown).

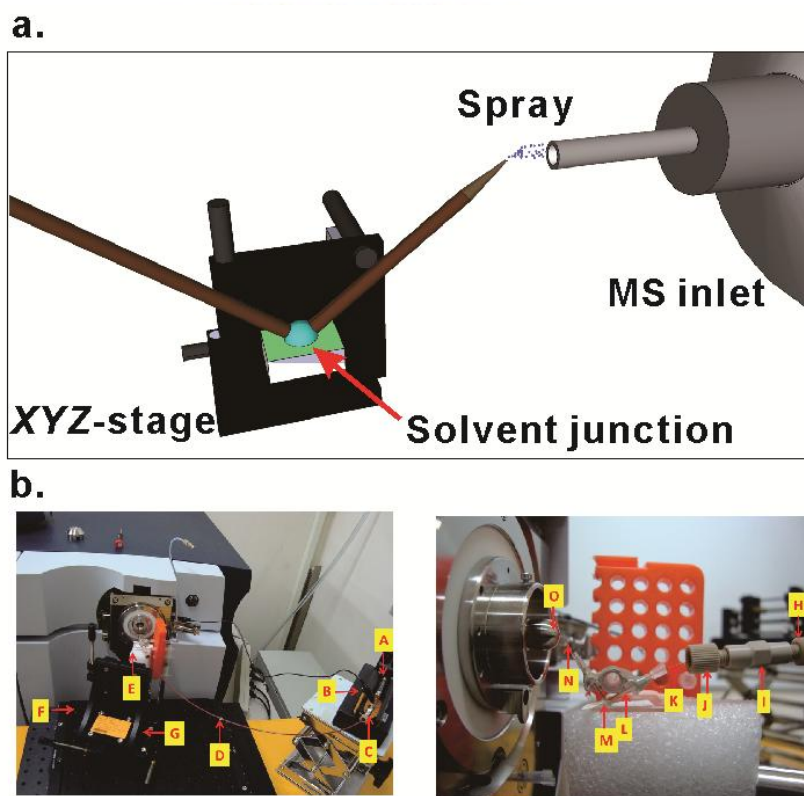


**Figure 3.1.** NanoDESI-MS setup used in this study. (a) 3D drawing of the setup (b) Photographs showing the assembly of the interface. Labels: (A) syringe, (B) grounding, (C) connector, (D) PEEK tubing, (E) sample stage, (F) one-axis stage, (G) XYZ-stage, (H) fitting, (I) connector, (J) fitting (K) solvent capillary, (L) plastic pipette tip, (M) solvent junction, (N) nanospray capillary, (O) MS inlet.

### 3.3.2 Testing the interface

After setting up the nanoDESI-MS interface, we tried to use it to detect standard chemicals, which are normally easily detected by common mass spectrometric methods. The

first compound analyzed was 9-aminoacridinine: 2  $\mu\text{L}$  of the standard solution ( $10^{-4}$  M, in acetone) was spotted on the surface of a glass slide, and dried. Thus, the total amount spotted was 2  $\mu\text{g}$ . The solvent system used in this nanoDESI experiment was composed of methanol and acetonitrile (1:1, v/v) spiked with acetic acid (final concentration,  $\sim 0.1\%$ ). The MS signal of protonated 9-aminoacridine was very high (**Figure 3.2a**).

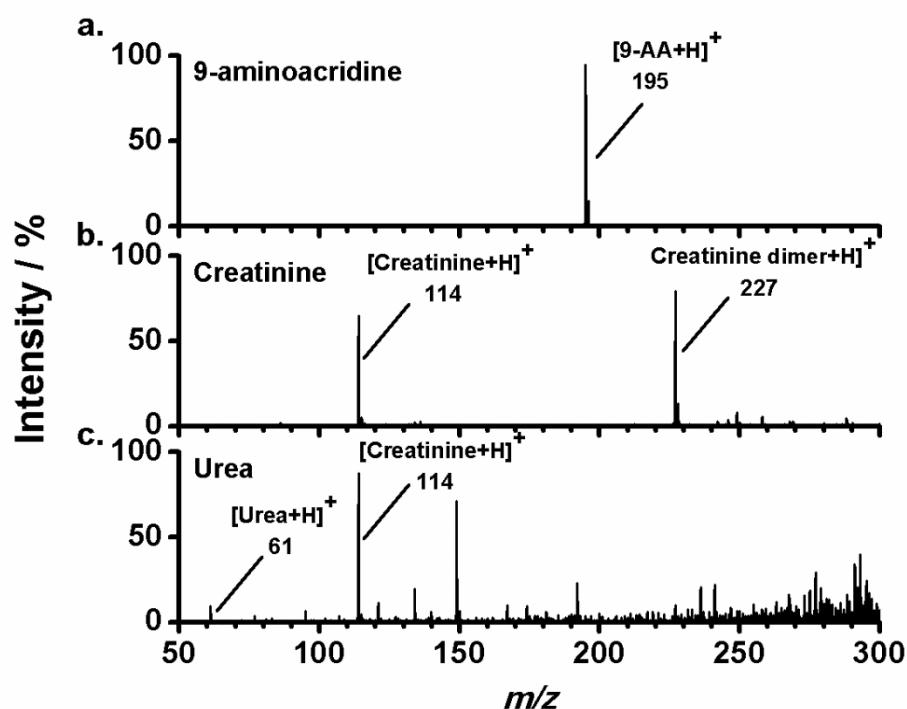


**Figure 3.2.** Testing the nanoDESI-MS setup with artificial samples. (a) Analysis of a dry 9-aminoacridine ( $m/z$  194) deposit on glass by nanoDESI-MS operated in the positive-ion mode. The sample was prepared in the following way: 2.0  $\mu\text{L}$  of  $10^{-4}$  M 9-aminoacridine solution in acetone were deposited on the tape, and dried. (b) Analysis of a dry creatinine ( $m/z$  113) deposit on glass by nanoDESI-MS operated in the positive-ion mode. The sample was prepared in the following way: 2.5  $\mu\text{L}$  of  $10^{-4}$  M creatinine solution in water were deposited on the glass, and dried. (c) Analysis of a dry urea ( $m/z$  60) deposit on glass by nanoDESI-MS operated in the positive-ion mode. The sample was prepared in the following way: 2.0  $\mu\text{L}$  of  $10^{-4}$  M urea solution in water were deposited on the glass, and dried. The solvent mixture used in this nano-DESI experiment was composed of methanol and acetonitrile in the volume ratio 1:1, and it was spiked with acetic acid (final concentration,  $\sim 0.1\%$ ).



Furthermore, using the nanoDESI-MS setup, we could readily detect creatinine and urea (**Figure 3.2b** and **3.2c**). In this experiment, we also noticed the problem of possible cross-contamination. For example, the spectrum in **Figure 3.2c** shows urea peak along with creatinine peak (which was present in the previously sample, **Figure 3.2b**).

### 3.3.3 Recording blank spectra of various solvent systems

We further evaluated quality of mass spectra recorded with different solvent systems, without depositing samples, in the negative-ion mode. We chose four different solvents for this study: (1) methanol/acetonitrile (1:1, v/v; with 0.1 % acetic acid); (2) methanol/acetonitrile (1:1, v/v); (3) acetonitrile; (4) methanol. Acetonitrile and acetic acid were LC-grade solvents, while methanol was LC-MS-grade solvent. The results are shown in **Figure 3.3**. We found that using the mixture of methanol and acetonitrile with acetic acid gave rise to a relatively high background feature in the  $m/z$  range of 170-300. Baselines obtained with other solvent systems were more flat. We think the LC-grade acetonitrile might contain more contaminants than other solvents; therefore, it contributes to the noisy background. Another source of spectral noise can be the acetic acid. We also found MS signals, which resemble those of polymers (peaks at the  $m/z$  171, 196, 221; **Figure 3.3**.) Therefore, polymers may also be extracted from plastic pipette tip, contributing to spectral noise in the negative-ion mode. Despite the high noise level – to our surprise – the methanol/acetonitrile (1:1, v/v; with 0.1 % acetic acid) system produced the best results with metabolite standards and real samples (see section 3.3.5). In the positive-ion mode, a signal suppression could be caused by the contaminant, was observed (see section 3.3.4).

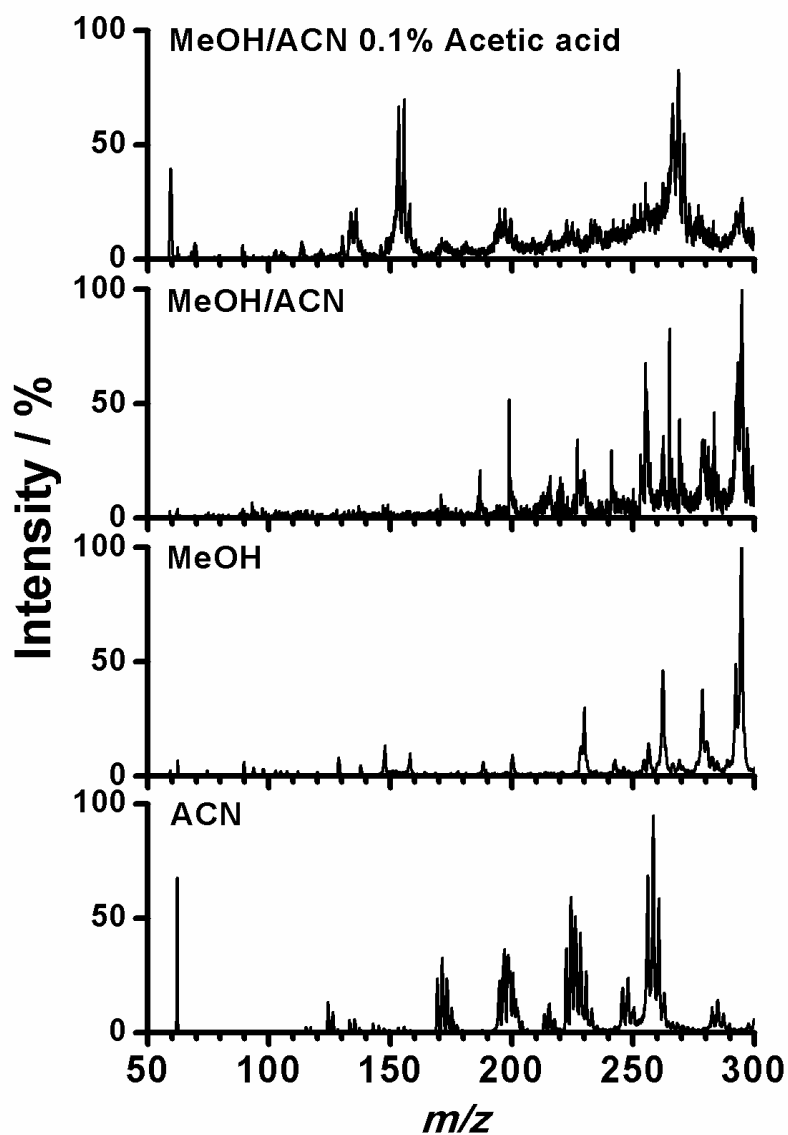


**Figure 3.3.** A blank nano-DESI mass spectrum recorded in the negative-ion mode; no sample target was present in the solvent junction area.

### 3.3.4 Comparison of various sampling materials

The goal of this experiment was to find a suitable material for sampling sweat from skin. We have tested five different materials (**Table 3.1**). The commercial plasters were most convenient because they have an adhesive layer and can be applied to human skin without safety concerns. Other materials tested (filter paper, Teflon) had other advantages, for

example, they have greater sorptive capabilities, or they are more resistant to solvents than the adhesive plasters.

We further carried out analysis of the sample targets (without samples present), which were chosen for sampling sweat directly from human skin (**Table 3.1**). Initially, we recorded a nanoDESI spectrum of a commercial plaster (A, *cf.* **Table 3.1**). As shown in **Figure 3.4**, spectral background in the positive-ion mode is quite strong. The high peak at the  $m/z$  149 is attributed to the common plasticizer: phthalic anhydride (molecular weight:  $148.1 \text{ g mol}^{-1}$ ). Another high peak, at the  $m/z$  145 can be attributed to polyethylene glycol present in the solvent mixture used. The high background is due to the high sensitivity of MS; in other words, even little quantities of contaminants cause high background. We also found that the plaster A gave high spectral background in the negative-ion mode (see section 3.3.4).

One important parameter of the sample support is the wettability of the surface by solvents. The glue-coated area of the plaster is hydrophobic; therefore, it is more compatible with the nanoDESI setup. When using the fabric area of the plaster for analysis, we found that the liquid bridge formed between the two capillaries was not stable, and much higher flow rates had to be used. In the positive-ion mode, a high spectral background was observed – in particular when using filter paper and Teflon tape as blank sample targets (**Figure 3.5**). In the positive-ion mode, most of the signals found in the spectra of plasters A, B and C essentially correspond to the solvent blank. However, in the negative-ion mode, we observed significant differences in the mass spectra recorded with different materials (**Figure 3.6**). Plaster A shows a spectral profile similar to the solvent spectrum recorded without any sample support (*i.e.* solvent blank). On the other hand, the analysis of plasters B and C yielded signals at the  $m/z$  121 and  $m/z$  165. Unfortunately, we could not identify the corresponding substances. Since plaster A relatively has a simple spectral background, we chose it for further work.

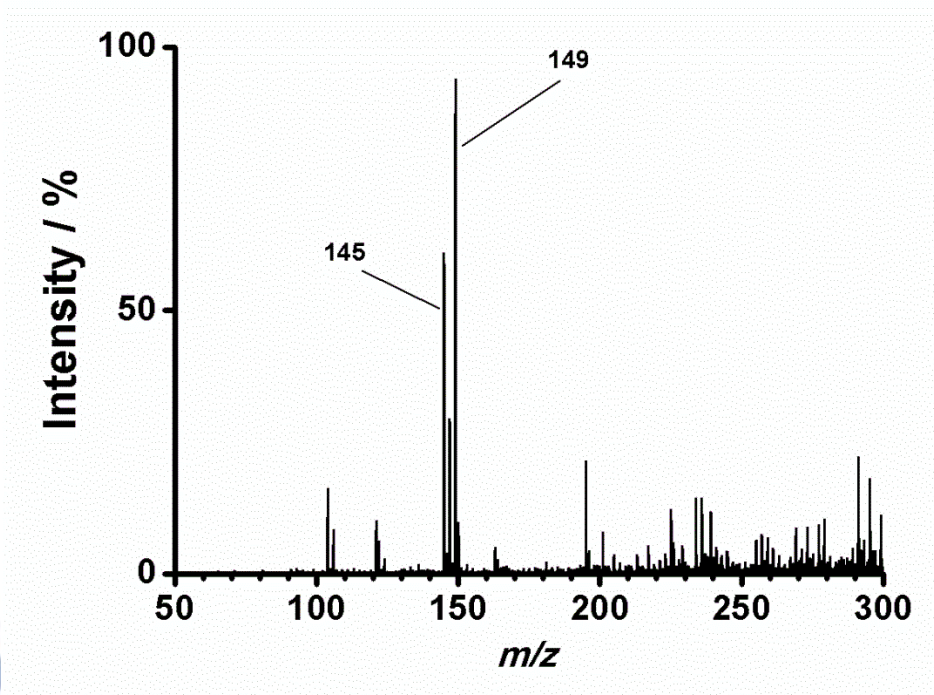


**Figure 3.4.** A positive-ion mode nano-DESI mass spectrum of plaster A (*cf.* **Table 3.1**). No sample has been deposited. The solvent mixture used in this nanoDESI experiment was composed of methanol and acetonitrile in the volume ratio 1:1, spiked with acetic acid (final concentration,  $\sim 0.1\%$ ). Several signals can be observed; for example, the peak at the  $m/z$  149 is most probably related to phthalic anhydride (molecular weight:  $148.1 \text{ g mol}^{-1}$ ), which is frequently used as plasticizer in consumer products.

The other materials tested appear to be less suitable sample supports for nanoDESI-MS operated in the negative-ion mode. Although these materials might have absorbed considerable volumes of sweat, they did not accommodate stable operation of the nanoDESI setup. In these cases, the liquid junction formed by the nanoDESI solvent was not stable due to a higher wettability as compared with the glue-coated plaster area. Therefore, we conclude that plaster A is a more compatible sampling material with the nanoDESI-MS system.



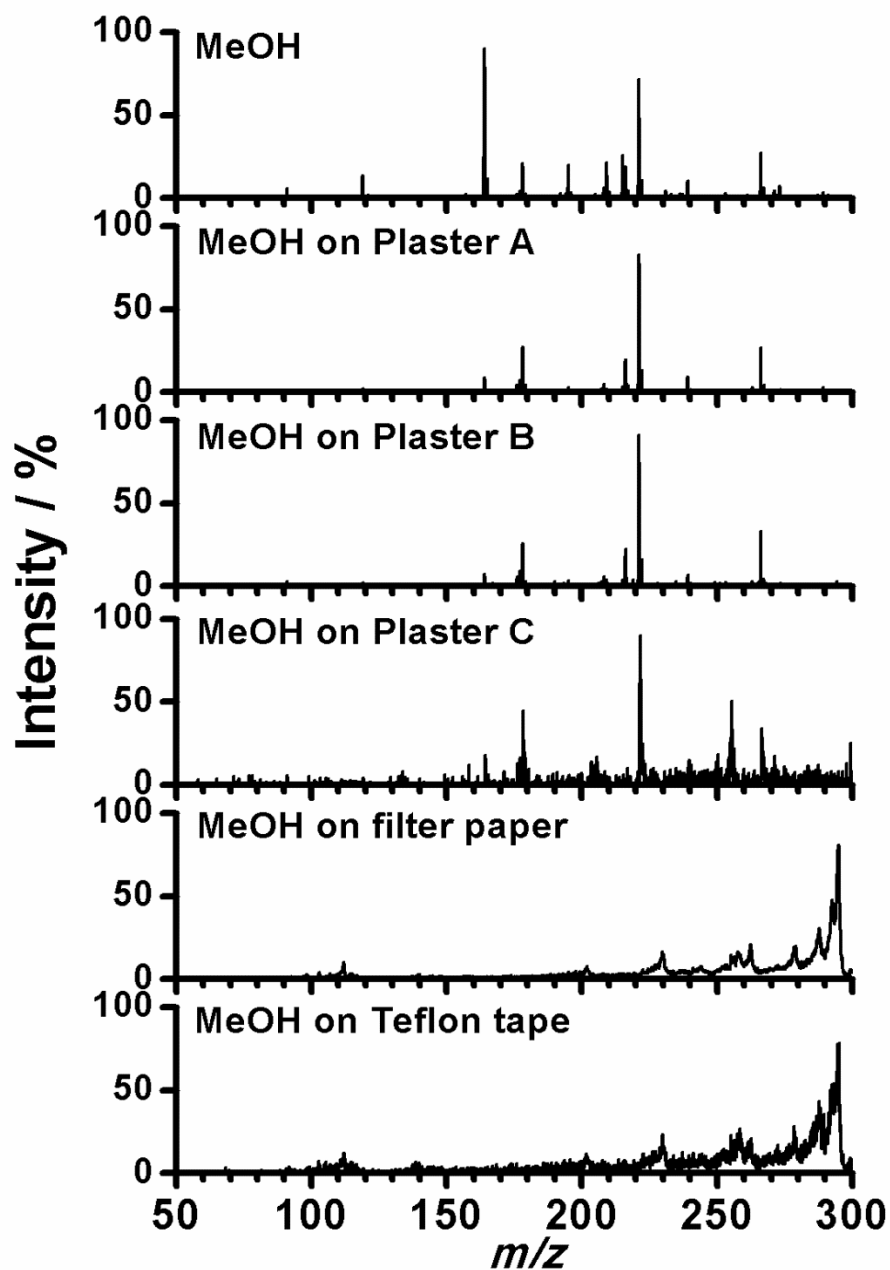


**Figure 3.5.** A blank nanoDESI mass spectrum recorded in the positive-ion mode; no sample target was present in the solvent junction area. The solvent used in this nanoDESI experiment was pure methanol (LC-MS grade). Comparison of different solvent systems used in nanoDESI experiments is presented in **Table 3.2**.

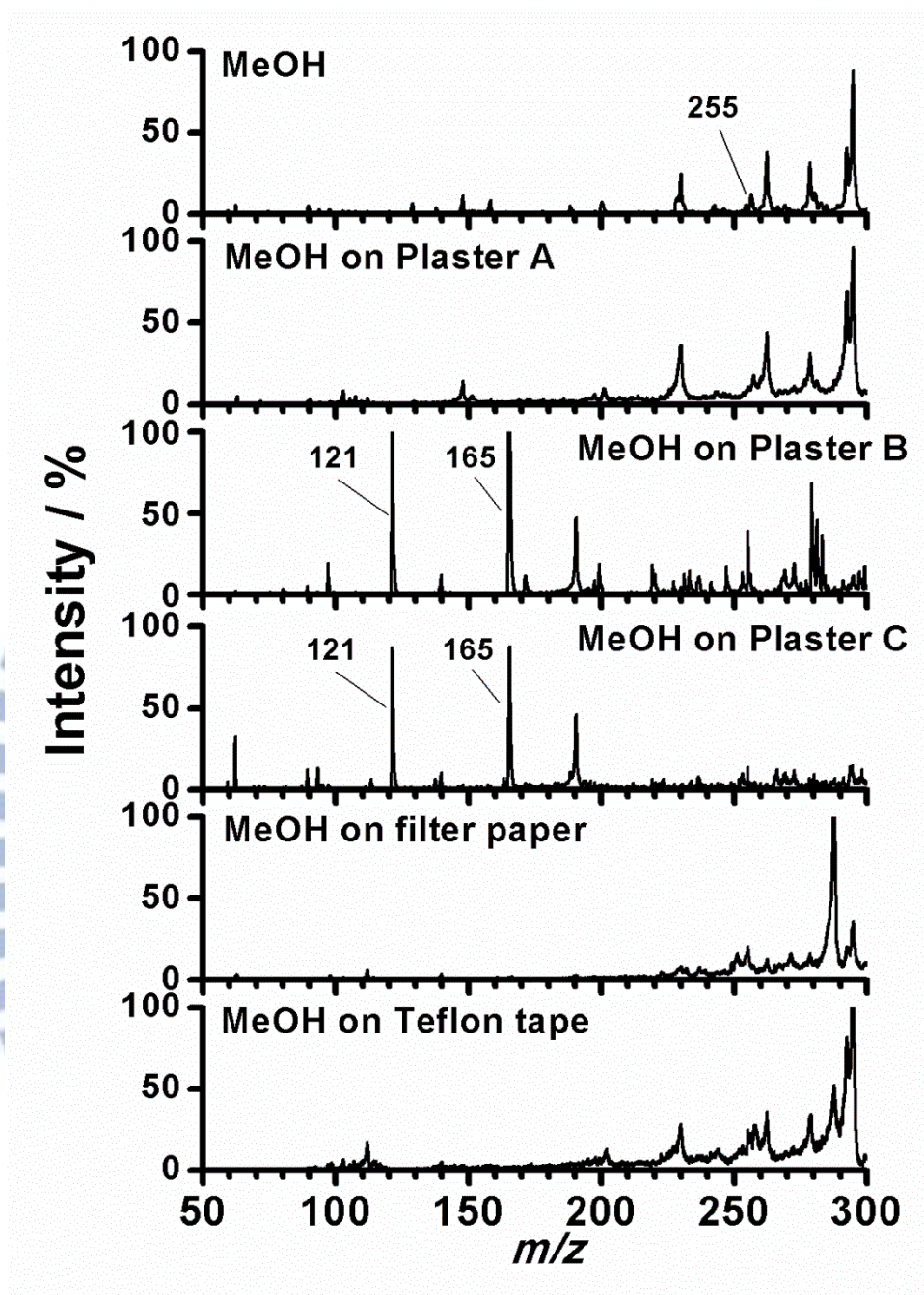


**Figure 3.6.** Comparison of negative-ion mode nanoDESI mass spectra obtained for various materials tested in this study. No samples were spotted. The solvent used in this nanoDESI experiment was pure methanol (LC-MS grade).

### 3.3.5 Analysis of a sweat sample

In the next experiment, we attempted using the nanoDESI-MS platform in the analysis of a real sample. A 2- $\mu$ L aliquot of the liquid sample was spotted on the plaster A, and it was dried before analysis. Subsequently, we placed the plaster A beneath the liquid junction of the nano-DESI interface. The solvent mixture used in this nanoDESI experiment was composed of methanol and acetonitrile in the volume ratio 1:1, and it was spiked with acetic acid (final concentration,  $\sim$  0.1%). **Figures 3.7** and **3.8** present the results obtained in the positive- and negative-ion modes, respectively.

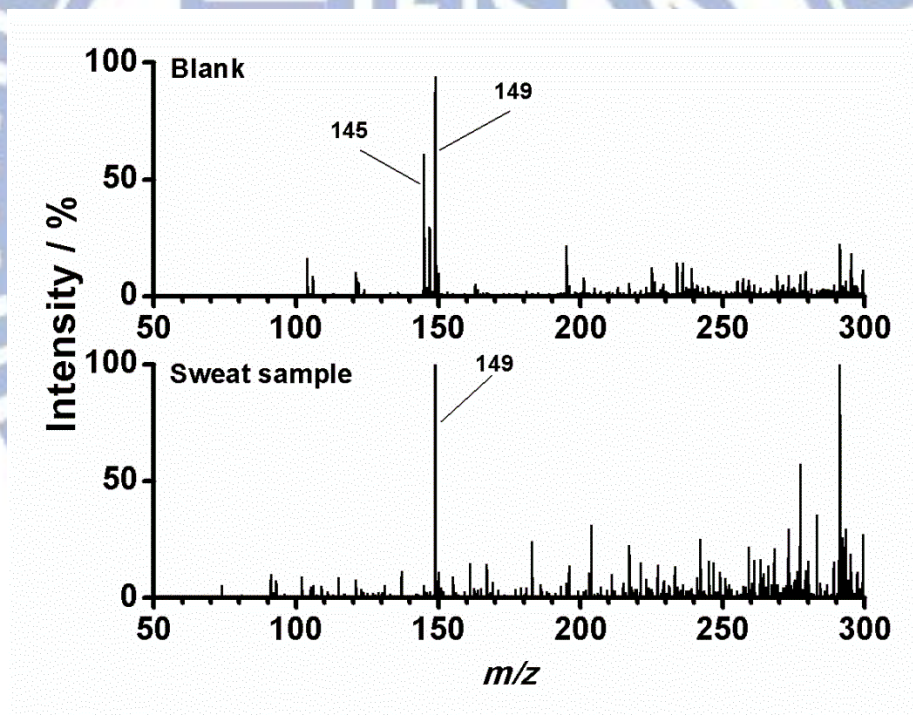


**Figure 3.7.** Analysis of a dry sweat deposit on plaster A by nanoDESI-MS operated in the positive-ion mode.

Initially, the sweat sample was centrifuged at 8000 rpm for 20 min, and subsequently filtered using a 0.2- $\mu$ m syringe filter. The solvent mixture used in this nanoDESI-MS experiment was composed of methanol and acetonitrile in the volume ratio 1:1, spiked with acetic acid (final concentration,  $\sim$  0.1%).

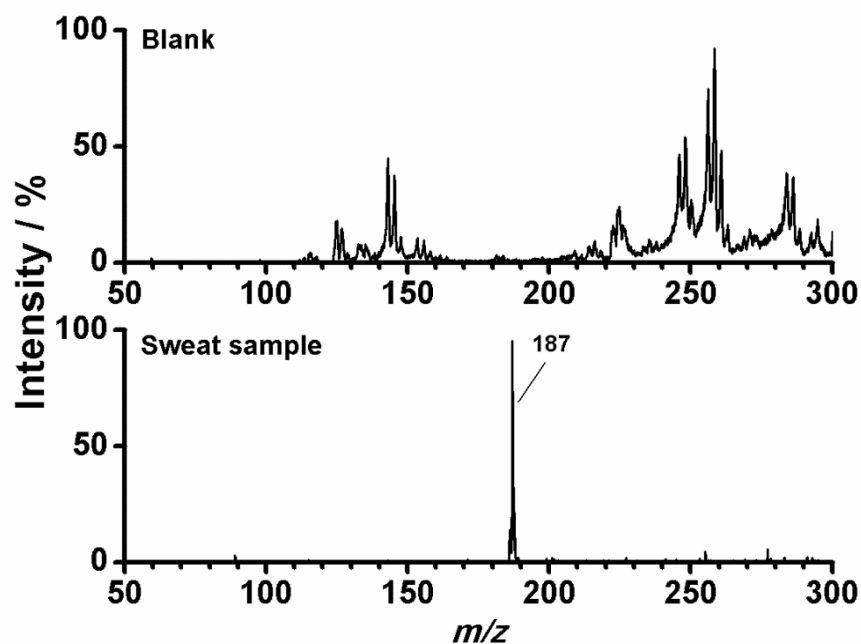


**Figure 3.8.** Analysis of a dry sweat deposit on plaster A by nanoDESI-MS operated in the negative-ion mode. Initially, the sweat sample was centrifuged at 8000 rpm for 20 min, and subsequently filtered using a 0.2- $\mu\text{m}$  syringe filter. The solvent mixture used in this nanoDESI-MS experiment was composed of methanol and acetonitrile in the volume ratio 1:1, spiked with acetic acid (final concentration,  $\sim 0.1\%$ ).

The MS signals from contaminants recorded in the positive-ion mode were relatively high. Some of the peaks present in these spectra cannot be found in the blank spectrum (*cf.* **Figure 3.4**), which suggests that these may be metabolites present in sweat. Nevertheless, we could not find the peaks corresponding to two metabolites which are normally abundant in sweat: urea and creatinine.<sup>69</sup> Interestingly, in the negative-ion mode, we could see a high peak at the  $m/z$  187. In an attempt to identify the corresponding metabolite, we carried out tandem MS analysis of this ion; however, we could not observe any significant fragment peaks even we amplify the drive level of Ion trap. Based on the a database search (Human Metabolome Database, Edmonton, Canada),<sup>70</sup> we suspect that this peak may correspond to *N*-acetyl-L-glutamine (molecular weight:  $188 \text{ g mol}^{-1}$ ), which is normally found in human



urine and is the acetylated form of the most abundant amino acid glutamine found in skeletal muscle tissue.<sup>71</sup> The intensities of other MS signals in the negative-ion mode were also higher than in the blank. However, due to possible overlap, based on the current data, it is hard to judge on the possibility to detect other metabolites. For example, a peak at the  $m/z$  255 appeared in the blank spectrum of pure methanol (**Figure 3.6**), and a relatively high peak at the same  $m/z$  was observed in the real sample. This peak could potentially be assigned to palmitic acid (molecular weight: 256 g mol<sup>-1</sup>). Overall, the high signal of *N*-acetyl-L-glutamine may suggest that (i) this compound is highly abundant in sweat, (ii) this compound has a high ionization efficiency in nanoDESI, or (iii) a combination of both.

In summary, we have demonstrated the feasibility of the analysis of sweat deposited on plaster by nanoDESI-MS. We have carried out optimization of solvent system, and pre-selected the sampling material. We have also analysed a real sample, deposited on adhesive plaster by nanoDESI-MS.

### 3.3.6 Direct sampling of sweat from skin followed by nanoDESI-MS

The next step in this project was an attempt to analyze metabolites sampled directly from skin (*i.e.* without the intermediate steps of collecting liquid samples, and pretreatment). The plaster was attached to skin of a volunteer for ~ 1 h: during this period, the metabolites secreted with sweat were supposed to adsorb on the glue-coated surface of the plaster A. The plasters were subsequently analyzed by nanoDESI-MS without further treatment. The solvent mixture used in this nanoDESI-MS experiment was composed of methanol and acetonitrile in the volume ratio 1:1, spiked with acetic acid (final concentration, ~ 0.1%). The quality of positive-ion spectra (**Figure 3.9**) was comparable to that in the previous experiment with sample pretreatment (**Figure 3.7**). For example, in one test, the volunteer who donated their

sweat samples drank a cup of coffee just before the sampling; however, we could not find the anticipated peak of caffeine at the  $m/z$  195 (**Figure 3.9**). On the other hand, in the negative-ion mode, a strong signal at the  $m/z$  187 was recorded (**Figure 3.10**). Other signals – which were observed in the blank spectra in the negative-ion mode (*cf.* **Figure 3.6**) – had lower intensity; most probably due to ion suppression. The signal-to-noise ratios of the peak at the  $m/z$  187, in the spectra obtained during the analysis of the liquid sample (**Figure 3.8**), and the “dry” sample collected directly on the plaster, were similar (**Figure 3.10**). Therefore, the basic concept of facile sampling (using passive samplers) used in conjunction with the nanoDESI-MS detection has been shown. However, further optimization of the sampling and the detection systems is necessary in order to detect not just one – but many – metabolites with high sensitivity.

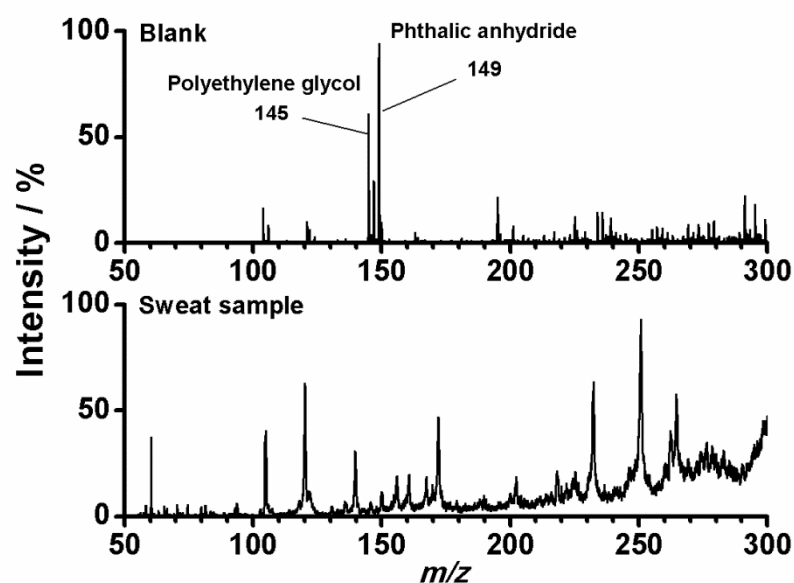


**Figure 3.9.** Analysis of a dry sweat collected directly on the plaster A by nanoDESI-MS operated in the positive-ion mode. The solvent mixture used in this nanoDESI-MS experiment was composed of methanol and acetonitrile in the volume ratio 1:1, spiked with acetic acid (final concentration, ~ 0.1%).

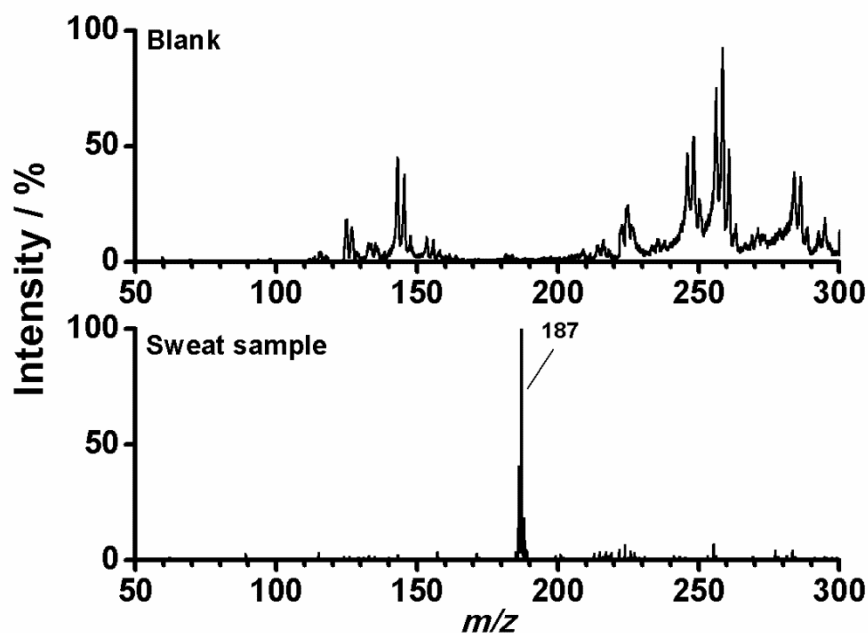


**Figure 3.10.** Analysis of a dry sweat collected directly on the plaster A by nanoDESI-MS operated in the negative-ion mode. The solvent mixture used in this nanoDESI-MS experiment was composed of methanol and acetonitrile in the volume ratio 1:1, spiked with acetic acid (final concentration,  $\sim 0.1\%$ ).

In an attempt to improve the quality of the mass spectra, we also tested pure methanol (LC-MS grade) as the nanoDESI solvent. Although the spectral background became lower, the sensitivity (as judged based on  $m/z$  187) also decreased (**Figure 3.11**). The knowledge – regarding spectral quality and sensitivity – gathered in this study – is presented in **Table 3.2**. Based on the current results, we advocate using the solvent mixture composed of methanol and acetonitrile in the volume ratio 1:1, spiked with acetic acid (final concentration,  $\sim 0.1\%$ ), as the nanoDESI solvent. We also suggest using high-purity (LC-MS) grade chemicals (acetonitrile, acetic acid) in future work. We conclude that the analysis of sweat samples by nano-DESI-MS combined with plaster-based sampling is more promising in the negative-ion mode than in the positive-ion mode.

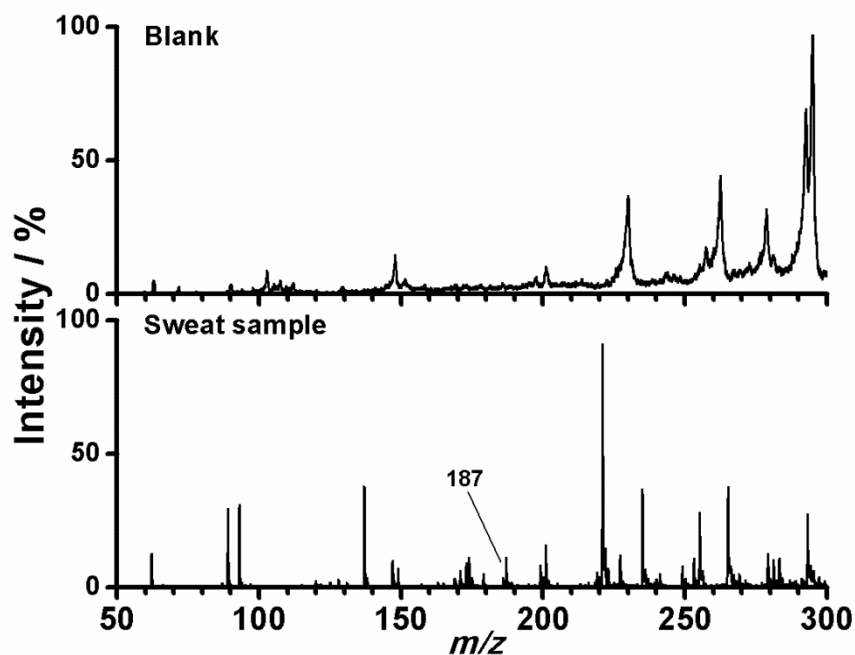


**Figure 3.11.** Analysis of a sweat sample on plaster A, following incubation of the plaster with skin of a volunteer, using nanoDESI-MS operated in the negative-ion mode. The solvent mixture used in this nanoDESI-MS experiment was pure methanol (LC-MS grade).

### 3.3.7 The influence of sampling time

In the final experiment, we evaluated the influence of sampling time on the signal-to-noise ratio. A series of samples were collected at varied sampling times: from 1 to 300 s. Interestingly, already after 10 s, a peak at the  $m/z$  187 could be recorded (**Figure 3.12**). The signal-to-noise ratio generally increased with the sampling time. The result confirms that sweat is secreted by skin all the time, and plaster patches can readily be used to collect samples of sweat from skin prior to the analysis by MS.



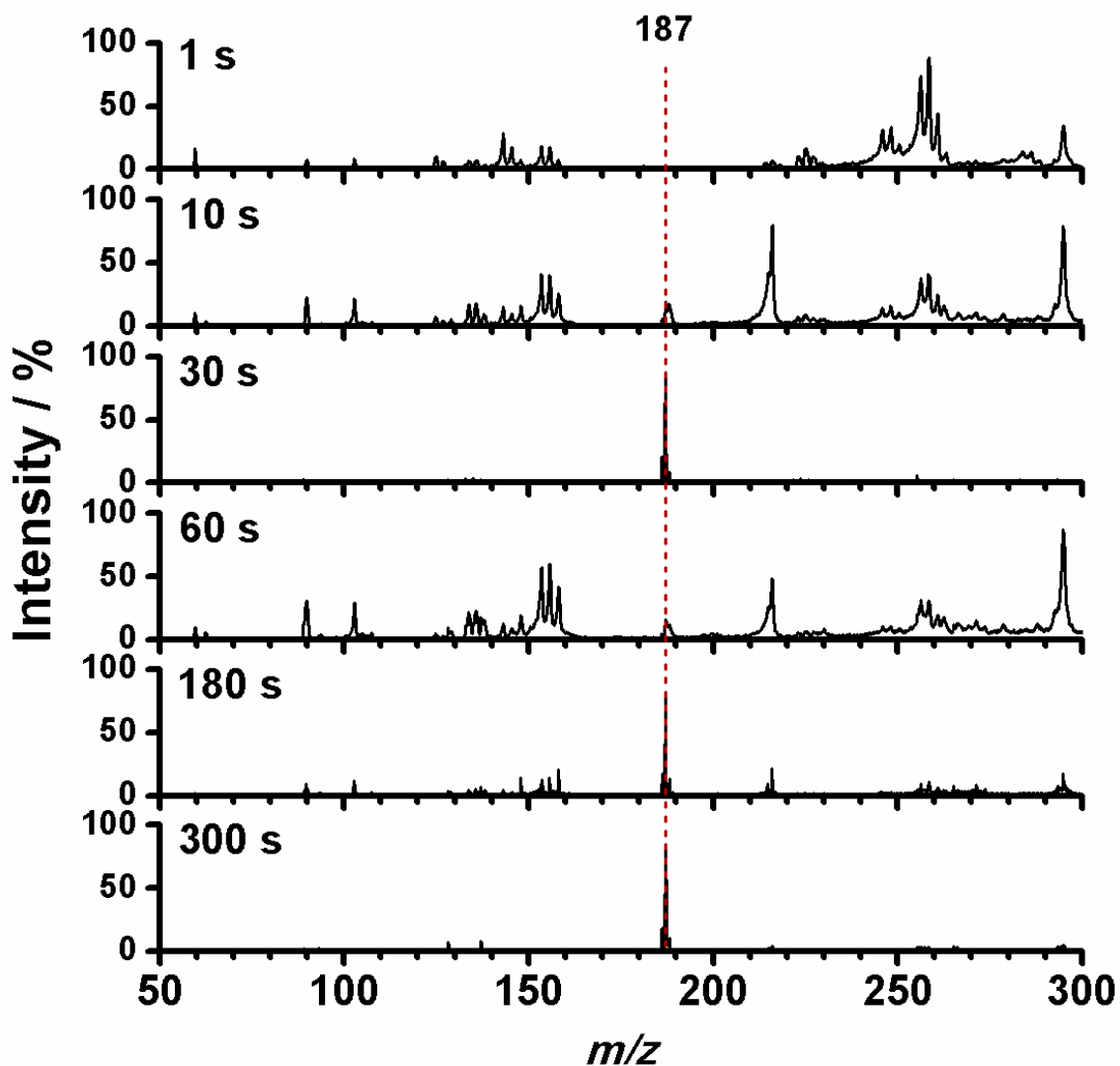


**Figure 3.12.** Analysis of a sweat sample on plaster A, following incubation of the plaster with skin of a volunteer, using nanoDESI-MS operated in the negative-ion mode. The sampling time was varied (1 – 300 s). The solvent mixture used in this nanoDESI-MS experiment was composed of methanol and acetonitrile in the volume ratio 1:1, spiked with acetic acid (final concentration, ~ 0.1%).

**Table 3.2.** Performance of various solvent systems tested in this study. The quality of baseline and sensitivity were judged based on series of experiments with standards/real samples. Methanol was LC-MS grade. Other solvents were LC grade.

Solvent	Baseline	Sensitivity
MeOH/Acetonitrile 0.1% acetic acid	+++	+++
MeOH/ACN	++	+
MeOH	+	++
Acetonitrile	++	+

### 3.4 Concluding remarks

In this work we have proposed application of adhesive plasters as sampling tools for sweat, and analysis of such samples by nano-DESI-MS. We have tested the home-made nanoDESI source using artificial samples, and found that the analyte peaks can readily be recorded by mass spectrometer. For example, creatine and urea could be detected in the dry sample deposits. We further optimized the way of collecting sweat samples as well as the key parameters of the nanoDESI-MS method in order to ensure satisfactory quality of mass spectra. The optimized parameters included: type of sampling material, nanoDESI solvent system, as well as the MS ion mode. It is noteworthy that the presented analytical method takes advantage of commercial plasters as simple sampling tools which enable facile collection of sweat samples. We have found that such plasters are also compatible with the nanoDESI-MS setup used as the main analytical platform. Signal of metabolite (*N*-acetyl-L-glutamine) could be detected by nanoDESI-MS following a very short sampling period (a few seconds). In future, one can apply this method to sweat analysis and further clinical diagnosis of sweat. The biggest problem observed during the development of this

method was a relatively high spectral background due to the contamination signals the solvent system or sampling plasters. To mitigate this problem high quality solvents adoption should be used in future work. Although commercial plasters are a convenient facilitating tool, they may also contribute to spectral background. To further develop this method, one needs to find or develop more reliable materials that would not increase the spectral noise, and could concentrate metabolites at the same time. In addition, one may consider using this simple sampling method with another ion source, for example direct analysis in real time (DART)<sup>72</sup> and easy ambient sonic-spray ionization EASI<sup>73</sup>.



# CHAPTER 4:

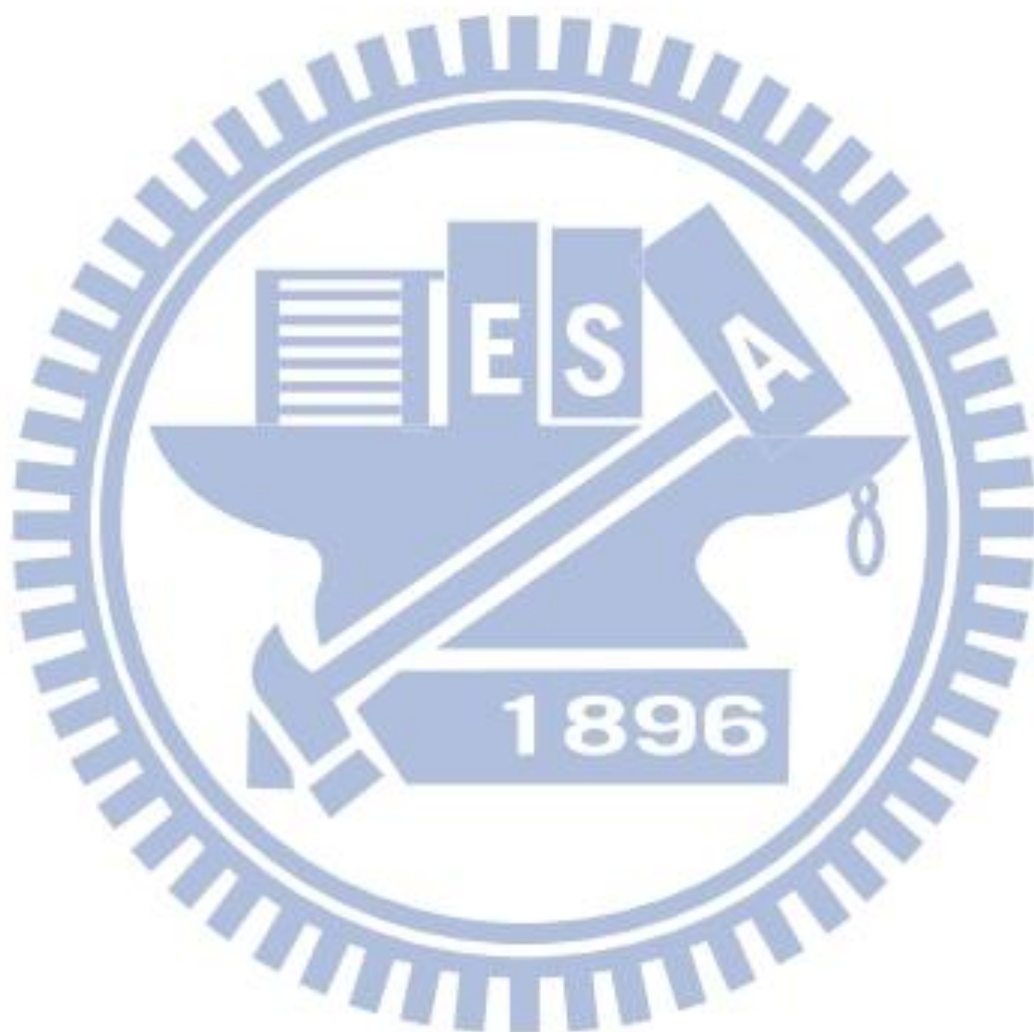
## Conclusions

---

This research work has led to the development of two methods for the analysis of metabolites in different kinds of biological samples by mass spectrometry. In the first study, we have developed a protocol for the analysis of small metazoan samples by matrix-assisted laser desorption/ionization mass spectrometry. The study has shown the feasibility of isotopic labeling of fruit flies with the purpose of pursuing metabolic effects of the circadian clock and environmental cues by mass spectrometry. The results also reveal a substantial metabolic inertia of the circadian clock: once adapted to the day/night cycle, the incorporation of  $^{13}\text{C}$  to UDP-Glc was not significantly altered by acute perturbation of the illumination cycle. We believe the method may also help to explore other biochemical phenomena in fruit fly as well as other metazoan species, which are commonly studied as model biological organisms. In the second part of this work, we have proposed application of adhesive plasters as sampling tools for sweat and subsequent analysis of such samples by nanospray desorption electrospray ionization. Following a short contact of plaster with skin (a few seconds), we could record one peak corresponding to a metabolite. The development of new sampling materials, which could reduce ion suppression and enhance sensitivity, is needed. If successful, in future, the method may find applications in analysis and doping control. Overall, the work shows a broad applicability of mass spectrometric platforms in the analysis of metabolites in biological



samples. We have successfully used mass spectrometry in the analysis of different kinds of samples (microscale biological specimens and sweat). This confirms that, mass spectrometry can play an important role in future discoveries in bioscience.



## References

1. Oldiges, M.; Lutz, S.; Pflug, S.; Schroer, K.; Stein, N.; Wiendahl, C., Metabolomics: current state and evolving methodologies and tools. *Appl Microbiol Biot* **2007**, *76*, 495-511
2. Fiehn, O., Metabolomics – the link between genotypes and phenotypes. *Plant Mol Biol* **2002**, *48* (1-2), 155-171.
3. Fiehn, O.; Kopka, J.; Dormann, P.; Altmann, T.; Trethewey, R. N.; Willmitzer, L., Metabolite profiling for plant functional genomics. *Nat Biotechnol* **2000**, *18*, 1157-1161.
4. Oldiges, M.; Kunze, M.; Degenring, D.; Sprenger, G. A.; Takors, R., Stimulation, monitoring, and analysis of pathway dynamics by metabolic profiling in the aromatic amino acid pathway. *Biotechnol Progr* **2004**, *20* (6), 1623-1633.
5. Fiehn, O.; Kopka, J.; Trethewey, R. N.; Willmitzer, L., Identification of uncommon plant metabolites based on calculation of elemental compositions using gas chromatography and quadrupole mass spectrometry. *Anal Chem* **2000**, *72*, 3573-3580.
6. Villas-Boas, S. G.; Hojer-Pedersen, J.; Akesson, M.; Smedsgaard, J.; Nielsen, J., Global metabolite analysis of yeast: evaluation of sample preparation methods. *Yeast* **2005**, *22*, 1155-1169.
7. Villas-Boas, S. G.; Mas, S.; Akesson, M.; Smedsgaard, J.; Nielsen, J., Mass spectrometry in metabolome analysis. *Mass Spectrom Rev* **2005**, *2*, 613-646.
8. Nielsen, J.; Oliver, S., The next wave in metabolome analysis. *Trends Biotechnol* **2005**, *23*, 544-546.
9. Mungur, R.; Glass, A. D. M.; Goodenow, D. B.; Lightfoot, D. A., Metabolite fingerprinting in transgenic *Nicotiana tabacum* altered by the *Escherichia coli* glutamate dehydrogenase gene. *J Biomed Biotechnol* **2005**, *2*, 198-214.
10. Allen, J.; Davey, H. M.; Broadhurst, D.; Heald, J. K.; Rowland, J. J.; Oliver, S. G.; Kell, D. B., High-throughput classification of yeast mutants for functional genomics using metabolic footprinting. *Nat Biotechnol* **2003**, *21*, 692-696.
11. Fuzfai, Z.; Katona, Z. F.; Kovacs, E.; Molnar-Perl, I., Simultaneous identification and quantification of the sugar, sugar alcohol, and carboxylic acid contents of sour cherry, apple, and berry fruits, as their trimethylsilyl derivatives, by gas chromatography-mass spectrometry. *J Agr Food Chem* **2004**, *52*, 7444-7452.
12. Buchholz, A.; Takors, R.; Wandrey, C., Quantification of intracellular metabolites in *Escherichia coli* K12 using liquid chromatographic-electrospray ionization tandem mass spectrometric techniques. *Anal Biochem* **2001**, *295*, 129-137.

13. Iwatani, S.; Van Dien, S.; Shimbo, K.; Kubota, K.; Kageyama, N.; Iwahata, D.; Miyano, H.; Hirayama, K.; Usuda, Y.; Shimizu, K.; Matsui, K., Determination of metabolic flux changes during fed-batch cultivation from measurements of intracellular amino acids by LC-MS/MS. *J Biotechnol* **2007**, *128*, 93-111.
14. Noh, K.; Gronke, K.; Luo, B.; Takors, R.; Oldiges, M.; Wiechert, W., Metabolic flux analysis at ultra short time scale: Isotopically non-stationary C-13 labeling experiments. *J Biotechnol* **2007**, *129*, 249-267.
15. Karas, M.; Hillenkamp, F., Laser Desorption Ionization of proteins with molecular masses exceeding 10000 daltons. *Anal Chem* **1988**, *60*, 2299-2301.
16. Zenobi, R.; Knochenmuss, R., Ion formation in MALDI mass spectrometry. *Mass Spectrom Rev* **1998**, *17*, 337-366.
17. Knochenmuss, R.; Zenobi, R., MALDI ionization: The role of in-plume processes. *Chem Rev* **2003**, *103*, 441-452.
18. Fenn, J. B.; Mann, M.; Meng, C. K.; Wong, S. F.; Whitehouse, C. M., electrospray ionization for mass-spectrometry of large biomolecules. *Science* **1989**, *246*, 64-71.
19. Wollnik, H., Time-of-Flight Mass Analyzers. *Mass Spectrom Rev* **1993**, *12*, 89-114.
20. Imrie, D. C.; Pentney, J. M.; Cottrell, J. S., A Faraday cup detector for high-mass ions in matrix-assisted laser desorption/ionization Time-of-Flight mass-spectrometry. *Rapid Commun Mass Spectrom* **1995**, *9*, 1293-1296.
21. Loboda, A. V.; Krutchinsky, A. N.; Bromirski, M.; Ens, W.; Standing, K. G., A tandem quadrupole/time-of-flight mass spectrometer with a matrix-assisted laser desorption/ionization source: design and performance. *Rapid Commun Mass Spectrom* **2000**, *14*, 1047-1057.
22. Paradisi, C.; Todd, J. F. J.; Traldi, P.; Vettori, U., Boundary effects and collisional activation in a quadrupole ion trap. *Org Mass Spectrom* **1992**, *27*, 251-254.
23. Stafford, G. C.; Kelley, P. E.; Syka, J. E. P.; Reynolds, W. E.; Todd, J. F. J., Recent improvements in and analytical applications of advanced ion trap technology. *Int J Mass Spectrom* **1984**, *60*, 85-98.
24. Nozue, K.; Covington, M. F.; Duek, P. D.; Lorrain, S.; Fankhauser, C.; Harmer, S. L.; Maloof, J. N., Rhythmic growth explained by coincidence between internal and external cues. *Nature* **2007**, *448*, 358-U11.
25. Mellow, M.; Spoelstra, K.; Roenneberg, T., The circadian cycle: daily rhythms from behaviour to genes - First in the Cycles Review Series. *Embo Rep* **2005**, *6*, 930-935.
26. Waterhouse, J.; Reilly, T.; Atkinson, G.; Edwards, B., Jet lag: trends and coping strategies. *Lancet* **2007**, *369*, 1117-1129.



27. Froy, O., Metabolism and circadian rhythms-implications for obesity. *Endocr Rev* **2010**, *31*, 1-24.
28. O'Neill, J. S.; Reddy, A. B., Circadian clocks in human red blood cells. *Nature* **2011**, *469*, 498-507.
29. Bae, K.; Edery, I., Regulating a circadian clock's period, phase and amplitude by phosphorylation: Insights from *Drosophila*. *J Biochem* **2006**, *140*, 609-617.
30. Adams, M. D. *et al.*, The genome sequence of *Drosophila melanogaster*. *Science* **2000**, *287*, 2185-2195.
31. Bier, E., *Drosophila*, the golden bug, emerges as a tool for human genetics. *Nat Rev Genet* **2005**, *6*, 9-23.
32. Shaw, P. J.; Cirelli, C.; Greenspan, R. J.; Tononi, G., Correlates of sleep and waking in *Drosophila melanogaster*. *Science* **2000**, *287*, 1834-1837.
33. Sehgal, A.; Mignot, E., Genetics of sleep and sleep disorders. *Cell* **2011**, *146*, 194-207.
34. Vanin, S.; Bhutani, S.; Montelli, S.; Menegazzi, P.; Green, E. W.; Pegoraro, M.; Sandrelli, F.; Costa, R.; Kyriacou, C. P., Unexpected features of *Drosophila* circadian behavioural rhythms under natural conditions. *Nature* **2012**, *484*, 371-U108.
35. Rubakhin, S. S.; Romanova, E. V.; Nemes, P.; Sweedler, J. V., Profiling metabolites and peptides in single cells. *Nat Methods* **2011**, *8*, S20-S29.
36. Svatos, A., Single-cell metabolomics comes of age: new developments in mass spectrometry profiling and imaging. *Anal Chem* **2011**, *83*, 5037-5044.
37. Hillenkamp, F.; Karas, M.; Beavis, R. C.; Chait, B. T., Matrix-assisted laser desorption ionization mass-spectrometry of biopolymers. *Anal Chem* **1991**, *63*, A1193-A1202.
38. Urban, P. L.; Schmidt, A. M.; Fagerer, S. R.; Amantonico, A.; Ibanez, A.; Jefimovs, K.; Heinemann, M.; Zenobi, R., Carbon-13 labelling strategy for studying the ATP metabolism in individual yeast cells by micro-arrays for mass spectrometry. *Mol Biosyst* **2011**, *7*, 2837-2840.
39. Hu, J. B.; Chen, Y. C.; Urban, P. L., On-target labeling of intracellular metabolites combined with chemical mapping of individual hyphae revealing cytoplasmic relocation of isotopologues. *Anal Chem* **2012**, *84*, 5110-5116.
40. Gouw, J. W.; Pinkse, M. W. H.; Vos, H. R.; Moshkin, Y.; Verrijzer, C. P.; Heck, A. J. R.; Krijgsveld, J., *In Vivo* stable isotope labeling of fruit flies reveals post-transcriptional regulation in the maternal-to-zygotic transition. *Mol Cell Proteomics* **2009**, *8*, 1566-1578.



41. Prasad, M.; Jang, A. C. C.; Starz-Gaiano, M.; Melani, M.; Montell, D. J., A protocol for culturing *Drosophila melanogaster* stage 9 egg chambers for live imaging. *Nat Protoc* **2007**, *2*, 2467-2473.
42. Rabinowitz, J. D.; Kimball, E., Acidic acetonitrile for cellular metabolome extraction from *Escherichia coli*. *Anal Chem* **2007**, *79*, 6167-6173.
43. Edwards, J. L.; Kennedy, R. T., Metabolomic analysis of eukaryotic tissue and prokaryotes using negative mode MALDI time-of-flight mass spectrometry. *Anal Chem* **2005**, *77*, 2201-2209.
44. Tsuboi, K. K.; Fukunaga, K.; Petricciani, J. C., Purification and specific kinetic properties of erythrocyte uridine diphosphate glucose pyrophosphorylase. *The Journal of biological chemistry* **1969**, *244*, 1008-15.
45. Parker, C. G.; Fessler, L. I.; Nelson, R. E.; Fessler, J. H., *Drosophila* Udp-glucose-glycoprotein glucosyltransferase – Sequence and Characterization of an enzyme that distinguishes between denatured and native proteins. *Embo J* **1995**, *14*, 1294-1303.
46. Sezgin, E.; Duvernell, D. D.; Matzkin, L. M.; Duan, Y. H.; Zhu, C. T.; Verrelli, B. C.; Eanes, W. F., Single-locus latitudinal clines and their relationship to temperate adaptation in metabolic genes and derived alleles in *Drosophila melanogaster*. *Genetics* **2004**, *168*, 923-931.
47. Stoleru, D.; Nawathean, P.; Fernandez, M. D. L. P.; Menet, J. S.; Ceriani, M. F.; Rosbash, M., The *Drosophila* circadian network is a seasonal timer. *Cell* **2007**, *129*, 207-219.
48. Peschel, N.; Helfrich-Forster, C., Setting the clock - by nature: Circadian rhythm in the fruitfly *Drosophila melanogaster*. *Febs Lett* **2011**, *585*, 1435-1442.
49. Rogulja, D.; Young, M. W., Control of sleep by cyclin A and its regulator. *Science* **2012**, *335*, 1617-1621.
50. Rothenfluh, A.; Abodeely, M.; Price, J. L.; Young, M. W., Isolation and analysis of six timeless alleles that cause short- or long-period circadian rhythms in *Drosophila*. *Genetics* **2000**, *156*, 665-675.
51. Grant, S. C.; Aiken, N. R.; Plant, H. D.; Gibbs, S.; Mareci, T. H.; Webb, A. G.; Blackband, S. J., NMR spectroscopy of single neurons. *Magnet Reson Med* **2000**, *44*, 19-22.
52. Kiessling, S.; Eichele, G.; Oster, H., Adrenal glucocorticoids have a key role in circadian resynchronization in a mouse model of jet lag. *J Clin Invest* **2010**, *120*, 2600-2609.
53. Riazanskaia, S.; Blackburn, G.; Harker, M.; Taylor, D.; Thomas, C. L. P., The analytical utility of thermally desorbed polydimethylsilicone membranes for in-vivo sampling of volatile organic compounds in and on human skin. *Analyst* **2008**, *133*, 1020-1027.

54. Delahunty, T.; Schoendorfer, D., Caffeine demethylation monitoring using a transdermal sweat patch. *J Anal Toxicol* **1998**, *22*, 596-600.
55. Kintz, P.; Brenneisen, R.; Bundeli, P.; Mangin, P., Sweat testing for heroin and metabolites in a heroin maintenance program. *Clin Chem* **1997**, *43*, 736-739.
56. Huang, C. T.; Chen, M. L.; Huang, L. L.; Mao, I. F., Uric acid and urea in human sweat. *Chinese J Physiol* **2002**, *45*, 109-115.
57. Gallagher, M.; Wysocki, J.; Leyden, J. J.; Spielman, A. I.; Sun, X.; Preti, G., Analyses of volatile organic compounds from human skin. *Brit J Dermatol* **2008**, *159*, 780-791.
58. Penn, D. J.; Oberzaucher, E.; Grammer, K.; Fischer, G.; Soini, H. A.; Wiesler, D.; Novotny, M. V.; Dixon, S. J.; Xu, Y.; Brereton, R. G., Individual and gender fingerprints in human body odour. *J R Soc Interface* **2007**, *4*, 331-340.
59. Takats, Z.; Wiseman, J. M.; Gologan, B.; Cooks, R. G., Mass spectrometry sampling under ambient conditions with desorption electrospray ionization. *Science* **2004**, *306*, 471-473.
60. Roach, P. J.; Laskin, J.; Laskin, A., Nanospray desorption electrospray ionization: an ambient method for liquid-extraction surface sampling in mass spectrometry. *Analyst* **2010**, *135*, 2233-2236.
61. Takats, Z.; Wiseman, J. M.; Cooks, R. G., Ambient mass spectrometry using desorption electrospray ionization (DESI): instrumentation, mechanisms and applications in forensics, chemistry, and biology. *J Mass Spectrom* **2005**, *40*, 1261-1275.
62. Talaty, N.; Takats, Z.; Cooks, R. G., Rapid in situ detection of alkaloids in plant tissue under ambient conditions using desorption electrospray ionization. *Analyst* **2005**, *130*, 1624-1633.
63. Laskin, J.; Heath, B. S.; Roach, P. J.; Cazares, L.; Semmes, O. J., Tissue imaging using nanospray desorption electrospray ionization mass spectrometry. *Anal Chem* **2012**, *84*, 141-148.
64. Ranc, V.; Havlicek, V.; Bednar, P.; Lemr, K., Nano-desorption electrospray and kinetic method in chiral analysis of drugs in whole human blood samples. *Eur J Mass Spectrom* **2008**, *14*, 411-417.
65. Wilm, M.; Mann, M., Analytical properties of the nanoelectrospray ion source. *Anal Chem* **1996**, *68*, 1-8.
66. Karas, M.; Bahr, U.; Dulcks, T., Nano-electrospray ionization mass spectrometry: addressing analytical problems beyond routine. *Fresen J Anal Chem* **2000**, *366*, 669-676.
67. Hsieh, C. H.; Chang, C. H.; Urban, P. L.; Chen, Y. C., Capillary action-supported

contactless atmospheric pressure ionization for the combined sampling and mass spectrometric analysis of biomolecules. *Anal Chem* **2011**, *83*, 2866-2869.

68. Kelly, R. T.; Page, J. S.; Luo, Q. Z.; Moore, R. J.; Orton, D. J.; Tang, K. Q.; Smith, R. D., Chemically etched open tubular and monolithic emitters for nanoelectrospray ionization mass spectrometry. *Anal Chem* **2006**, *78*, 7796-7801.
69. Harker, M.; Coulson, H.; Fairweather, I.; Taylor, D.; Daykin, C. A., Study of metabolite composition of eccrine sweat from healthy male and female human subjects by H-1 NMR spectroscopy. *Metabolomics* **2006**, *2*, 105-112.
70. Wishart, D. S. *et al.*, HMDB: the human metabolome database. *Nucleic Acids Res* **2007**, *35*, 521-526.
71. Magnusson, I.; Kihlberg, R.; Alvestrand, A.; Wernerman, J.; Ekman, L.; Wahren, J., Utilization of intravenously administered *N*-acetyl-L-glutamine in humans. *Metabolism* **1989**, *38*, 82-88.
72. Cody, R. B.; Laramée, J. A.; Durst, H. D., Versatile new ion source for the analysis of materials in open air under ambient conditions. *Anal Chem* **2005**, *77*, 2297-2302.
73. Haddad, R.; Sparrapan, R.; Kotiaho, T.; Eberlin, M. N., Easy ambient sonic-spray ionization-membrane interface mass spectrometry for direct analysis of solution constituents. *Anal Chem* **2008**, *80*, 898-903.